Spatiotemporal variability of Canadian High Arctic glacier surface albedo from MODIS data, 2001-16

Colleen A. Mortimer[1] and Martin Sharp[1]

[1]Department of Earth and Atmospheric Sciences, University of Alberta, Edmonton, T6G 2E3, Canada

Correspondence to: Colleen A. Mortimer (cmortime@ualberta.ca)

Abstract. Inter-annual variations and longer-term trends in the annual mass balance of glaciers in Canada's Queen Elizabeth Islands (QEI) are largely attributable to changes in summer melt. The largest source of melt energy in the QEI in summer is net shortwave radiation, which is modulated by changes in glacier surface albedo. We used measurements from the Moderate Resolution Imaging Spectroradiometer (MODIS) sensors to investigate ~~large~~ large-scale spatial patterns, ~~and~~ temporal trends, and variability in the summer surface albedo of QEI glaciers ~~and their relationship to observed changes in glacier surface temperature~~ from 2001 to 2016. Mean summer black-sky shortwave broadband albedo (BSA) decreased at a rate of 0.029 ± 0.025 decade^{-1} over that period. Larger reductions in BSA occurred in July (-0.050 ± 0.031 decade^{-1}). No change in BSA was observed in either June or August. Most of the decrease in BSA, which was greatest at lower elevations around the margins of the ice masses, occurred between 2007 and 2012 when mean summer BSA was anomalously low. The First Principal Component of the 16-year record of mean summer BSA was well correlated with the mean summer North Atlantic Oscillation Index, except in 2006, 2010, and 2016 when the mean summer BSA appears to be dominated by the August BSA. During the period 2001–16, ~~this 16-year period,~~ the mean summer LST increased by 0.~~046~~ 049 ± 0.~~036~~ 038 °C yr^{-1} and the BSA record was negatively correlated (r: -0.~~64~~86, ~~p<0.01~~) with the LST record, indicative of a positive ice-albedo feedback that would increase rates of mass loss from the QEI glaciers.

1 Introduction

The area of glaciers and ice caps in the Queen Elizabeth Islands (QEI, Fig. 1), Arctic Canada, in 2000 was ~104,000 km^2 (Arendt et al., ~~2013~~2012). From 2000 to 2015, the summer mean surface temperature of glaciers in this region increased at a rate of 0.06 ± 0.04°C yr^{-1}, and summer mean air temperatures from 2005-~~20~~12 were > 1.0°C warmer than the 1948-2015 mean (Mortimer et al., 2016). QEI summer mean air and glacier surface temperatures are strongly correlated with the annual and summer glacier mass balances, which have become increasingly negative since at least 2003 (Gardner et al., 2013; Lenaerts et al., 2013; Wolken et al., 2016). Inter-annual variations and longer-term trends in annual glacier mass balance in the QEI are dominated by changes in summer melt (Koerner, 2005), and net shortwave radiation is the largest source of melt energy on

Commented [CM1]: Rev 1
RC 1 Title: consider removing "C6" from the title since it's not t
different from C5 for the albedo and LST, and many people, befo
reading the paper, have no idea what C6 is. You have appropriate
mentioned the fact that you've used C6 in the paper as needed.
Also consider including LST in the title, especially if you decide
enhance the discussion about cause-and-effect between LST and
albedo for the QEI.
AR 1: Reference to "C6" removed from the title.

Commented [m2]: Rev. 1
RC 5: Line 14: note that the range of years says 2008-2012 on li
486
AR 5: Corrected to read 2007-2012 throughout.

the QEI ice caps (Gascon et al., 2013). Variability in net shortwave radiation, in turn, is strongly modulated by changes in the surface albedo (van den Broeke et al., 2011; Tedesco et al., 2016), the ratio of reflected to incoming solar radiation.

The high albedo of fresh snow declines naturally over time due to settling and grain growth (Warren, 1982). This initial decrease in albedo raises the shortwave energy absorption, leading to warming and/or melt, and a further lowering of the surface albedo. Warmer temperatures and increased snowpack water content further accelerate grain growth, causing more rapid albedo decline that enhances surface warming and/or melt (Wiscombe and Warren, 1980; Colbeck, 1982). A positive snow/ice albedo feedback has been linked to accelerating high-latitude warming, and is increasingly recognized as an important factor in explaining recent increases in rates of mass loss from the Greenland Ice Sheet (e.g. Tedesco et al., 2016), which lies immediately to the east of the QEI.

On glaciers and ice caps, surface warming and increased melt in summer can lead to earlier and more widespread removal of the previous winter's snowpack, and earlier and more prolonged exposure of underlying low-albedo glacier ice. Albedo decreases can also be caused by aerosol deposition (Warren and Wiscombe, 1980), ~~enhanced~~ biological activity on glacier surfaces (Fountain et al., 2004), and ~~accelerated~~ the release of impurities from melting snow and ice, which become concentrated at the snow/ice surface (Clarke and Noone, 1985; Conway et al., 1996; Flanner et al., 2007; Doherty et al., 2010). Given the observed increases in air and glacier surface temperatures across the QEI (Mortimer et al., 2016) we anticipate a reduction in the surface albedo in this region, unless warming has also been accompanied by an increase in solid precipitation (Vincent et al., 2015) that is large enough to raise the surface albedo (e.g. Box et al., 2012). The expected albedo reduction has, however, yet to be documented or quantified.

Decadal-scale declines in the surface albedo of the Greenland Ice Sheet~~, which lies immediately to the east of the QEI,~~ have been simulated using regional climate models, and documented using remote sensing data validated by in situ measurements (e.g. Stroeve et al., 2005, 2013; Box et al., 2012; 2017; Alexander et al., 2014; Tedesco et al., 2016; Casey et al. 2017~~Stroeve et al., 2005, 2013; Casey et al. 2017; Box et al., 2012; 2017; Alexander et al., 2014; Tedesco et al., 2016).~~ Global assessments of land surface albedo (e.g. He et al., 2014) have included the QEI, but these analyses were extremely broad in nature and the detailed spatial pattern of glacier albedo change and its variation over time are unknown. Between 2000 and 2015, measured increases in both QEI summer 700 hPa air from the NCEP/NCAR R1 Reanalysis (Kalnay and others, 1996) and glacier surface temperatures from the Moderate Resolution Imaging Spectroradiometer (MODIS) ~~and glacier surface temperatures in the QEI~~ were greatest in the north and west of the ~~region~~ QEI (Sharp et al., 2011; Mortimer et al., 2016). ~~but w~~We do not know whether there is a similar spatial pattern in the albedo record.

Field-based measurements provide information about the surface albedo at specific locations, but there are no long-term spatially distributed in-situ records of the surface radiation budget of glaciers and ice caps in the QEI.

Remote sensing methods enable monitoring of the surface albedo and its spatial and temporal variability at the scale of both individual ice caps and the regional glacier cover. Here, we use measurements of surface albedo from the ~~Moderate Resolution Imaging Spectroradiometer (~~MODIS~~)~~ sensors to present the first near-complete picture of variations in the summer surface albedo of QEI glaciers and ice caps from 2001 to 2016. We characterize the spatial and temporal variability in summer albedo,

Commented [m3]: Rev. 2
RC 13: Page 2, line 38 – What is meant by 'accelerated release'? Suggestion to reword, clarify intent.
AR 13: Sentence reworded.

Commented [m4]: Rev. 2
RC 14: Page 2, lines 40-42 – The authors are correct to state fres snow would raise surface albedo. Suggestion to include QEI precipitation data quantifying the suggestion, or reference precipitation studies.
AR 14: Reference to Vincent et al. (2015) has been added. Vince al. (2015) found an increase in both total precipitation as well as increase in the ratio of snowfall to total precipitation over the Canadian Arctic during the period 1948-2012. These trends were calculated by gridding climate station data. In the QEI, there are three such stations (Resolute Bay, Eureka, Alert) and none are located over ice. Reference to Box et al. (2012) which found a second-order negative albedo feedback (positive correlation betw albedo and surface air temperature anomalies) in the accumulatio area of the nearby Greenland Ice Sheet has also been added to the of this sentence.

Commented [m5]: Rev. 2
RC 15: Page 2, line 49 – Suggestion to clarify for readers the sou of the temperature analysis used in referenced studies.
AR 15: clarification added.

and quantify the rate of albedo change across the QEI~~, and investigate spatial patterns in the relationship between the mean summer albedo and mean summer land surface temperature (LST) records over the QEI ice caps and glaciers from 2001 to 2016.~~

2 Data and methods

2.1 MCD43A3 data

Observations from the ~~Moderate Resolution Imaging Spectroradiometers (~~MODIS sensors~~)~~, aboard the Terra (2000 to present) and Aqua (2002 to present) satellites (Barnes et al., 1998), are used to assess the spatial and temporal evolution of the surface albedo over the QEI glaciers and ice caps in summer (June-August). We use the MODIS/Terra and Aqua BRDF/Albedo Daily L3 Global – 500m Collection 06 (C6) product (MCD43A3, Schaaf and Wang (2015)), which provides both white-sky (bi-hemispherical reflectance under isotropic conditions) and black-sky (directional hemispherical reflectance) shortwave broadband surface albedo (Schaaf et al., 2011; https://www.umb.edu/spectralmass/terra_aqua_modis/v006, and references therein). MCD43A3 albedo is calculated daily for local solar noon ~~from~~ using atmospherically corrected surface reflectance measurements ~~from~~ made by sensors on both the Terra and Aqua satellites over a 16-day period that is centered on the ninth day of each 16-day moving window (https://www.umb.edu/spectralmass/terra_aqua_modis/v006). A semi-empirical Bidirectional Reflectance Distribution Function (BRDF) model, which describes the surface scattering/reflectance of a target as a function of illumination, is used to estimate surface albedo from directional surface reflectance information recorded by the MODIS sensors (Schaaf et al., 2002, 2011; Jin et al., 2003; Salomon et al., 2006). MCD43A3 white- and black-sky albedos are estimated from Level 2G-lite surface reflectances (MOD/MYD 09) for seven visible and near-infrared bands (spanning 0.4 to 2.4 µm) and three broad bands (shortwave (0.3-5.0 µm), visible (0.3-0.7 µm) and near infrared (0.7-5.0 µm)) in one of two ways.

If sufficient (>7) multi-date cloud-free observations with angular sampling sufficient to fully characterize the viewing/illumination geometry are acquired during a ~~16~~ 16-day period, a high quality *full inversion* is run using a semi-empirical RossThick LiSparse Reciprocal (RTSLR) kernel-driven BRDF model (Wanner et al., 1997; ~~Lutch~~ Lucht et al., 2000; Schaaf et al., 2002~~,~~; ~~201b~~2011). If insufficient observations (<7) are available, then a lower quality *magnitude inversion*, which relies on a priori knowledge to scale an archetypal BRDF, is used to estimate the surface albedo (Strugnell and Lutch, 2001; Schaaf et al., 2002; Jin et al., 2003; Liu et al., 2009). Data quality flags, provided in the MCD43A2 data quality assessment product, indicate whether albedo values [for each pixel] were obtained using the *full* or *magnitude inversion*. Since this study aims to generate an initial assessment of the spatio-temporal variability of the surface albedo of glaciers and ice caps in the QEI with good spatial coverage, both *full* and *magnitude inversion* data are used. Although *magnitude inversions* produce lower quality albedo estimates than the *full inversion* method, previous work using the C5 data showed that the *magnitude*

Commented [m6]: Rev. 1
RC 6 Line 60: MODIS has already been defined on lines 53 & 54
AR 6: Corrected.

Commented [m7]: Rev 1
RC 7 Line 76 & 78: Lutch should be spelled Lucht
AR 7: Misspelled reference corrected.

inversion data provide a good representation of the seasonal and spatial patterns ~~in~~ of glacier surface albedo (Schaaf et al., 2011; Stroeve et al., 2013). To our knowledge, no recent research comparing the *magnitude* and *full inversion* retrievals over glaciers and ice caps has been published for the MCD43A3 C6 data. Comparison of the MODIS C5 and C6 *full inversion* albedo data from the Greenland Ice Sheet confirmed many of the broad spatial patterns in surface albedo identified in the C5 data, but the magnitude of the C6 albedo change was much smaller (Casey et al., 2017).

2.1.1 MODIS sensor degradation

The MODIS sensors are currently operating well beyond their expected [productive] six year lifetimes (Barnes et al, 1998; Justice 1998) and the detectors are degrading (Xiong et al., 2001). For both the MODIS Terra and Aqua sensors, instruments were calibrated pre-launch (radiometric, spatial, specular calibration) (Gunther et al., 1996). On-orbit calibration procedures were included to monitor the sensor degradation that is expected as the instruments are exposed to solar radiation (Gunther et al., 1996). For the reflective solar bands (0.41–2.2 µm) the onboard calibration system includes a solar diffuser (SD) calibrated using the solar diffuser stability monitor (SDSM) (Gunther et al., 1998). Lunar and Earth view observations (select desert sites) are also used to assess radiometric stability (Sun et al. 2003). Even so, long-term scan mirror and wavelength dependent degradation which are not sufficiently accounted for by the on-board calibrators (SD/SDMS) have been observed (Xiong et al., 2001; Lyapustin et al., 2014 and references therein). Calibration degradation effects, which are largely confined to the MODIS Terra sensor, are greatest in the blue band (B3) and decrease with increasing wavelength (Xiong and Barnes 2006). An anomaly in the SD door operation (3 May 2003) and a decision to leave the door permanently open, exposing the SD to additional solar radiation, resulted in degradation of the SD on the MODIS Terra sensor that was faster than had originally been anticipated, and than was observed for the MODIS Aqua sensor (Xiong et al., 2005). Differences in the response versus scan angle (RVS) for the two side mirrors were also characterized pre-launch (Barnes et al., 1998). The RVS is important because it describes the scan mirror's response to different angles of incidence (AOI, for each band, detector and mirror side) (Sun et al., 2014). However, for the MODIS Terra sensor, following an overheating incident during pre-launch calibration, the RVS was not re-characterized and the exact pre-launch RVS characteristics are not known (Pan et al., 2007; Sun et al., 2014 and references therein). These issues have resulted in the performance of the MODIS Terra sensor being poorer than that of the MODIS Aqua sensor.

As a normal part of the operational procedure, the MODIS Characterization Support Team (http:mcst.gsfc.nasa.gov) periodically updates the calibration algorithms and approaches, during which time the entire L1B record (calibrated top of the atmosphere radiances) is re-processed to reflect improved understanding and characterization of changes to the instruments. Even so, non-physical trends in MODIS Terra data products, that result from calibration drift, have been observed and are well documented (e.g. Xiong et al., 2001; Xiong and Barnes, 2006; Franz et al., 2008; Kwiatkowski et al., 2008; Wang et al., 2012; Lyapustin et al., 2014; and references therein). The latest revision occurred with the C6 data and includes on-orbit calibration procedures to mitigate long-term calibration drift, particularly at the shorter wavelengths (Wenny et al., 2010; Toller et al.,

Commented [m8]: Rev. 2
RC 20: The paragraph (Page 4, Paragraph 3) could be rewritten t more informative and clear regarding MODIS sensor design and capabilities.
AR 20: MODIS Characterization Support Team literature has be reviewed and this section has been re-written to be more informa

Commented [m9]: Rev. 2
RC 16: Page 4, line 98 – Delete 'some of'.
AR 16: Deleted 'some of'

Commented [m10]: Rev. 1
RC 8 Line 99: perhaps the word "detectors" should be used inste of "instruments"??
AR 8: The word "instruments" replaced by "detectors".

Commented [m11]: Rev. 2
RC 17: Page 4, line 102 – Lyapustin et al. was not the first to rep on Terra's band degradation. Recommendation to additionally re and cite early / appropriate work, e.g. Xiong et al., 2001, Degrad of MODIS optics and its reflective solar bands calibration, doi: 10.1117/12.450646
AR 17: References to earlier studies have been added.

Commented [m12]: R2: Page 4, line 102 – Lyapustin et al. not the first to report on Terra's band degradation. Recommendat to additionally read and cite early / appropriate work, e.g. Xiong al., 2001, Degradation of MODIS optics and its reflective solar b calibration, doi: 10.1117/12.450646
Xiong and Barnes, 2006, An overview of MODIS radiometric calibration and characterization, doi: 10.1007/s00376-006-0008
Sun et al., 2014 Time-dependent response versus scan angle for MODIS reflective solar bands, IEEE TGRS, doi: 10.1109/TGRS.2013.2271448

2013; Sun et al., 2014; Lyapustin et al., 2014). The C6 dataset uses the on-board calibrators (e.g. SD/SDMS) and the mirror side ratios from lunar standard and Eearth view observations (Toller et al, 2013; Sun et al., 2014). The C6 revision also includes an additional approach, aimed primarily at the short-wavelength bands, that uses observations of desert sites (pseudo-invariant targets) to derive instrument calibration coefficients and RVS at multiple ~~angles of incidence~~AOIs (instead of the two AOIs provided by the SD and lunar standard) (Toller et al, 2013; Sun et al., 2014). Although this vicarious approach is less accurate than the one that uses the mirror-side ratios calibrated using a lunar standard, it has been found to provide a significant improvement to the L1B radiance measurements relative to the C5 data, prior to ~2013 (Toller 2013; Lyapustin et al., 2014). Updated L1B C6 radiances can be up to several percent higher than the C5 values (e.g. Band 3 and for most recent period ~2013 onward) (Toller et al., 2013; Lyapustin et al. 2014; Casey et al., 2017). However, evaluation of the L1B C6 Band 3 (0.46-0.48 µm) radiance over a desert site (Libya 4) identified residual errors (decadal trends on the order of several tenths of 1%; Lyapustin et al., 2014) that are within the product's stated accuracy (2% in absolute reflectance units for the reflective solar bands (Barnes et al., 1998; Justice et al., 1998)). The impact of the C6 updates on higher level MODIS science products is difficult to quantify because the corrections are time, mirror-side, angular, and detector dependent (Toller et al., 2013; Lyapustin et al. 2014; Sun et al., 2014). In addition, the C6 revision includes updates to algorithms (in addition to the calibration updates) used in the derivation of specific higher-level products (https://www.umb.edu/spectralmass/terra_aqua_modis/v006 outlines changes made to the MCD43A3 C6 data product). Important for the current study, however, is that recent analysis of surface albedo over the Greenland Ice Sheet, immediately to the east of the QEI, using MODIS C6 data (including the MCD43A3 product used in this study) identified statistically significant albedo declines over the wet snow zone (Casey et al., 2017). For the most part, these declines are thought to be physically real (Casey et al., 2017), which gives us confidence in the albedo trends presented here. ~~t~~There are no long-term, spatially distributed, in situ albedo records from the glaciers and ice caps in the QEI, so a comparison. This is both a motivation for, and a limitation of, the current study.

Furthermore, the MCD43A3 data used here were produced only under clear sky conditions (Hall et al., 2002; 2012). A conservative cloud mask is applied to remove observations made when clouds are detected (Ackerman et al., 1998). The resulting data gaps may introduce variability in the albedo record that is not representative of true physical change. Despite this, the MCD43A3 albedo product has been found to provide a reasonable representation of the seasonal albedo cycle over glaciers and ice caps (e.g. Stroeve et al., 2006). Hence, in the absence of long-term ground measurements of glacier surface albedo in the QEI, we made the assumption that this is also the case in the QEI.

~~The principal uncertainties in MODIS-derived surface albedo data arise from cloud contamination and sensor degradation. Similarity in the spectral signatures of snow, ice, and thin cloud makes it difficult to discriminate between these surface types (Strabala et al., 1994; King et al., 2004), and the conservative MODIS cloud mask tends to detect more clouds than actually occur over snow and ice (Ackerman et al., 1998; Hall et al., 2008a). Thus, the absence of observations for periods when clouds are present and the removal of data for periods when clouds are detected may introduce variability in the albedo record that is not representative of true physical change. Despite this, the MCD43A3 albedo product has been found to provide a reasonable representation of the seasonal albedo cycle over glaciers and ice caps (e.g. Stroeve et al., 2006). Hence, in the absence of long-~~

Commented [m13]: Rev. 2
RC 18: Page 4, paragraph 3. Suggestion for authors to reread literature on MODIS sensor calibration, degradation and capabili Line 110, more correct to state that C6 did improve radiance measurements from launch to ~2013. It remains to be assessed ho accurate and reliable MODIS C6 data will be moving forward fro C6 implementation (~2013 to present). Line 110: Recommendat to check the MODIS Characterization Support Team literature https://mcst.gsfc.nasa.gov/publications?f%5Btype%5D=102 .
AC 18: Literature has been reviewed and note about improved radiances up until ~2013 has been added.

Commented [m14]: Rev. 2
RC 19: For lines 113-114, it is not that the sensor is capable of identifying trends greater than 0.01, so much as +/- 0.01 is the lin of MODIS sensor accuracy and precision. The paragraph could b rewritten to be more informative and clear regarding MODIS sen design and capabilities.
AC 19: This paragraph has been re-written to be more informativ and accurate regarding MODIS sensor design and capabilities. Th text *'is capable of identifying trends greater than 0.01'* has been removed.

Commented [m15]: Rev. 2
RC 16: Page 3, lines 89-91 – Suggestion to edit sentences. As written, one could glean that it is difficult to discriminate betwee surface snow and ice vs cloud spectral visible-thermal infrared response. This is not always difficult to do spectrally. If the autho intend to discuss cloud remote sensing only, please clarify this. A more appropriate reference than Hall 2008a, may be Hall et al., 2 MODIS snow-cover products, Remote Sensing of Environment, 181-194.
AR 16: text moved and re-written for clarity. Reference to Hall 2 has been added. The issue of concern here is the absence of cloud which can potentially introduce additional variability in the datas that is not representative of physical changes on the surface.

term ground measurements of glacier surface albedo in the QEI, we made the assumption that this is also the case in that region.

The MODIS sensors are currently operating well beyond their expected [productive] six year lifetimes and some of the instruments are degrading (Wang et al., 2012; Toller et al., 2013). Systematic (decreasing) temporal trends are present in measurements in the visible and NIR (bands 1-7) of the MODIS C5 data (Lyapustin et al., 2014). Calibration degradation effects, which are largely confined to the Terra sensor, are greatest in the blue band (B3) and decrease with increasing wavelength (Lyapustin et al., 2014). Over time, un-corrected sensor degradation gives rise to decreasing measured surface radiances, which may result in apparent MODIS-derived albedo declines that differ from the true physical change. Contrary to the findings of earlier work that identified strong albedo declines over the dry snow zone of the Greenland Ice Sheet from 2001-2013 using the C5 data (e.g. Stroeve et al., 2005, 2013; Box et al., 2012; Alexander et al., 2014), a recent investigation concluded that much of the observed decline in broadband albedo from Terra-only data resulted from sensor degradation (Polashenski et al., 2015).

Long-term drifts in sensor calibration are addressed in the C6 data used in this study. A new calibration technique that uses in-orbit data from pseudo time-invariant desert site targets is in the calculation of C6 surface reflectances (Toller et al., 2013). This vicarious calibration approach has improved the precision of C6 reflectances, and it also mitigates long-term sensor drift, particularly at the shorter wavelengths. The C6 post-calibration residual error is on the order of several tenths of one percent for top-of the atmosphere (TOA) reflectance (Lyapustin et al., 2014), but larger discrepancies between calibrated Aqua and Terra measurements have been observed in the most recent data (post 2014) (Casey et al., 2017). MODIS C6 data have been shown to be capable of identifying trends in surface albedo >0.01 decade^{-1} (Lyapustin et al., 2014). A recent analysis of summer (June-August) ice surface albedo changes from MODIS C6 data identified statistically significant declines in surface albedo over the wet snow zone of the Greenland Ice Sheet during the period 2001-2016. For the most part, these decreases in surface albedo are thought to be physically real (Casey et al., 2017).

There are no long-term, spatially distributed, in situ albedo records from the glaciers and ice caps in the QEI, so a comparison between the MCD43A3 records and ground observations is not possible, and this is a limitation of this study. Ground-truthing of the MOD10A1 C6 albedo product over the Greenland Ice Sheet, immediately adjacent to the QEI, has been undertaken using in situ measurements from the Greenland Climate Network (GC-Net) and the Programme for Monitoring of the Greenland Ice Sheet (PROMICE) (Box et al., 2017). This study found the MOD10A1 C6 data to be a reasonable representation of the true surface albedo. In the absence of quality spatially distributed field measurements of surface albedo from our study area, we assume that this is also the case on the QEI ice caps.

Commented [m16]: Rev. 2
RC 2: "In the data and methods section (Page 4, line 122) MOD10A1 data was mentioned "to be a reasonable representatio the true surface albedo". Does this refer to analysis conducted by authors for this manuscript or to Box et al., 2017? Please clarify. MOD10A1 data was not inspected by the authors for this manusc why not?"
AC 2: The reference to the MOD10A1 data has been removed an the methods section detailing MODIS sensor calibration issues ha been revised.

Commented [m17]: Rev 1
RC 9 Line 120-124: this discussion of MOD10A1 should be dele it is not relevant to this paper, and MOD10A1 is never mentioned again in the paper; it really isn't good validation for MCD43A3
AR 9: Discussion of MOD10A1 has been deleted. Additionally, response to an anonymous reviewer's comments, this section has been revised to be more informative regarding MODIS sensor de and capabilities.

2.~~1~~ 1.2 MCD43A3 data processing

Summer (1-2 June (day 152) to 30-31 August (day 243)) MODIS MCD43A3 and MCD43A2 C~~ollection~~ 6 (Schaaf and Wang, 2015) data for MODIS tiles h17v00, h16v00, h16v01, and h15v01 for the period 2001-2016 were obtained from the NASA/USGS Land Processes Distributed Active Archive Center (Schaaf and Wang (2015), http://lpdaac.usgs.gov/ accessed November 2016). Daytime clear-sky white- and black-sky shortwave broadband ~~and visible albedo~~ data (MCD43A3) and accompanying quality assessment information (MCD43A2) were extracted from the hierarchical data format files and re-projected from the standard MODIS sinusoidal projection to a North America Albers Equal Area projection, WGS84 datum, 500 m resolution, using the MODIS re-projection tool version 4.1 (https://lpdaac.usgs.gov/tools/modis_reprojection_tool). The maximum summer (June-August) solar zenith angle over our study area (74°) was below the product's stated accuracy (<75°, Vermote et al., 2011; Wang et al., 2012), so no additional filtering was performed to remove data with high solar zenith angles. The white- and black sky albedos (representing completely diffuse and completely direct illumination, respectively) represent extreme estimates of the actual (blue-sky) bi-hemispheric surface albedo. To avoid redundancy, only results for the black-sky albedo (BSA) (which are fully consistent with those obtained using the white-sky albedo (WSA)) are presented here. The BSA was selected because our analysis focuses on albedo retrieved under clear-sky conditions. This approach is consistent with previous work using MCD43A3 data (e.g. Alexander et al., 2014; Tedesco et al., 2016; Casey et al., 2017). Unless ~~otherwise specified, henceforth BSA refers to the shortwave broadband black-sky albedo.~~

2.2 MODIS LST (MOD11A2)

Warmer surface temperatures increase the rates grain metamorphism and snowmelt, resulting in larger snow grains which have a lower albedo than those of fresh snow (Wiscombe and Warren 1980; Colbeck 1982) (Sect. 1.0). Air and surface temperatures also affect the timing of removal of the seasonal snowpack, which exposes lower albedo firn or glacier ice. Additionally, the melt of glacier ice releases impurities that have a low albedo and thus change the surface albedo of both ice and snow (e.g. Clarke and Noone 1985; Doherty et al., 2010; Sect. 1.0). As such, analysis of the glacier surface temperature and comparison of these data with the albedo record is included to help understand the observed spatiotemporal patterns of glacier albedo change in the QEI.

We use t~~T~~he Eight-Day L3 Global Land Surface Temperature and Emissivity product (MOD11A2) ~~C5~~C6, which has been found to be a reasonable proxy for the duration and/or intensity of summer melting in the QEI (Sharp et al., 2011; Mortimer et al., 2016), ~~was used~~ to investigate the relationship between glacier surface temperature and albedo. Only the 'daytime' LST data, generated with the day/night algorithm of Wan and Li (1997), is evaluated here. This is consistent with previous work in this region (e.g. Sharp et al., 2011, Mortimer et al. 2016). MOD11A2 daytime and night-time LSTs are computed from MODIS channels 31 (11 µm) and 32 (12 µm) using a split-window technique and all available daytime clear-sky scenes from the Terra satellite for sequential eight day periods (Wan et al., 2002). These data have a spatial resolution of 1 km and nominal product accuracy of ± 1°C but the accuracy over snow and ice surfaces can be as low as ±2°C (Hall et al., 2008~~zb~~; Koenig and Hall,

Commented [m18]: Rev. 2
RC 21: Page 5, line 129 – Suggestion to move citation to correct location in the sentence, i.e. Schaaf and Wang 2015 reference sho immediately follow MCD43 product mention.
AR: citation moved.

Commented [m19]: Rev. 2
RC 22: Page 5, line 141 – Awkward as written, suggestion to rev to clarify further use of BSA term e.g. 'henceforth BSA refers to black sky albedo MODIS shortwave broadband data.'
AR 22: Line no longer included in manuscript.

Commented [CM20]: Rev 1.
RC: Though they point out that albedo and LST are negatively correlated for the QEI, they do not discuss that relationship as ca and-effect in either the Abstract or the Conclusion. The relationsh between albedo and LST is discussed in Section 4.2 but I would l liked that discussion to have been better integrated throughout th paper.

Commented [m21]: Rev. 2
RC 4: "Section 2.2 discusses MODIS LST data. Why was Collec 5 MOD11A2 data used? (Page 5, lines 155-157) Communication with the MODIS data distributor, LP DAAC, revealed that MOD11A2 and MYD11A2 Collection 6 data have been available since mid-2015. Additionally, with the discussion of the Terra se degradation, it seems short-sighted to use Terra data only. Why w Terra data used? Was Aqua data used (i.e. MYD11A2)? If not, w not? Recommendation to add MYD11A2 data analysis."
AR 4: The manuscript has been revised and now uses the C6 MOD11A2 data instead of the C5 product. Terra data was used because of the time period under investigation with Terra data be since 2000 and Aqua data only being available since 2002. The T data allowed comparison with the albedo record for the full time period (2001-16).

2010). The LST analyses presented here are an update of those presented by Mortimer et al. (2016) which used ~~the~~ MODIS C5 data. The two analyses also differ in the time period used (we use 2001-16 instead of 2000-15 to coincide with the BSA analysis). Pixels for which the average LST error (QC_Day LST error flag) exceeded 2°C were removed from the analysis and any remaining pixels having a temperature >0°C were assigned a temperature of 0°C (e.g. ~~Hall et al., 2008a;~~ Mortimer et al., 2016). Uncertainties in trends derived from the MOD11A2 LST data ~~in the MOD11A2 LSTs~~ arise mainly from cloud contamination (Box et al., 2012; Hall et al., 2012) and the removal of observations for periods when clouds are detected (Ackerman et al., 1998; Hall et al., 2008ba). Variability in the number of clear-sky days within each observation period and from one year to the next was not found to introduce significant variability in the MODIS-derived LST relative to the true near-surface air temperature in the QEI (see Mortimer et al., 2016). MOD11A2 C6 data were downloaded from (https://lpdaac.usgs.gov/, accessed September 2014 - October 2015 and June 2017) and re-projected to a North America Albers Equal Area projection, WGS84 datum, 1 km resolution.

2.3 Mean summer BSA and LST

Annual precipitation in the QEI is low (<400 mm yr^{-1}) and varies little from one year to the next~~.~~; i~~I~~n contrast, the annual temperature range is large (> 40°C) (Braithwaite, 2005). Inter-annual variability in QEI annual mass balance is dominated by changes in the summer mass balance (Koerner, 2005), which, in turn, is strongly correlated with summer air temperature (Sharp et al., 2011). Spatial and temporal patterns in BSA and LST were, therefore, evaluated for the summer months (June-August). For each year during the 2001-~~20~~16 period, mean summer (JJA) BSA was calculated for pixels having at least 10 BSA observations in each month (June, July, August) and at least 45 of a possible 92 observations during the JJA period. These monthly thresholds ensure both an even distribution of BSA data throughout the summer season and consistency between different years. Mean summer LST was calculated following the methods of Mortimer et al. (2016) where the mean summer LST is calculated for pixels having at least 7 of a possible 12 observations between 1-2 June (day 153) and 28-29 August (day 241).

The m~~M~~ean summer (JJA) BSA and LST and the mean monthly (June, July, August) BSA, as well as the BSA and LST anomalies, ~~anomalies~~ were calculated on a pixel-by-pixel basis relative to the 2001-~~20~~16 mean for pixels having mean summer observations in 11 or more years. ~~This~~ These constituted ~87% and ~~93~~98% of possible BSA and LST pixels, respectively. Long-term rates of change in BSA and LST over the period 2001-~~20~~16 were determined by linear regression between the 16 year records of mean summer LST ~~and~~/ BSA and time. Consistent with the BSA and LST anomalies, regressions were computed on a pixel-by-pixel basis for all pixels having mean summer observations for 11 or more years. Following Casey et al. (2017), BSA trends between -0.001 yr^{-1} and +0.001 yr^{-1} are considered to be negligible. Negligible trends were defined by Casey et al. (2017) on the basis of the magnitude of the residual calibration uncertainties in the C6 data (on the order of several tenths of one percent in TOA reflectance (Lyaputsin et al., 2014)) over pseudo-invariant desert sites (Sect. 2.1.1). ~~albedo trends below the detection limit of the C6 data (0.01 $decade^{-1}$ (Lyapustin et al., 2014)) are considered to be negligible.~~

Commented [m22]: Rev. 2
RC 11: Recommendation for the authors to clearly state the additional QEI LST analysis provided in this manuscript as comp to Mortimer et al., 2016.
AR 11: Following your recommendations, the manuscript has be revised and now includes the MOD11A2 C6 data instead of the C data. Text has been added to the Methods (Section 2.2) to clearly state the differences in the QEI LST analysis provided in this manuscript compared to Mortimer et al., 2016.

Commented [m23]: Rev. 1
RC 10.1: Hall et al. (2008a) did not remove pixels with errors >2 C that were below zero, if I am recalling correctly.
AR 10.1: You are correct in pointing out that Hall et al. 2008a di not remove pixels with errors >2°C that were below 0°C. Hall et (2008a) developed melt-frequency maps and identified any pixels with a LST >0°C as experiencing melt. The inclusion of Hall et a (2008a) at the end of this sentence is, as you say, incorrect and misleading. As such, the reference to Hall et al. 2(008a) has been removed and only the reference to Mortimer et al. (2016) is inclu
RC 10.2: …'it's impossible to have a temperature greater than ze and still be ice.':
AR 10.2: Although the temperature of pure ice and snow cannot exceed 0°C, many pixels are not comprised solely of pure ice and snow. Rock, dust, impurities and ponded water (for which the maximum temperature can exceed 0°C) can exist on the snow/ice surface. The presence of these materials within the 1km x 1km pi can result in an LST >0°C. Mortimer et al. (2016) found that pixe having an LST >0°C were mainly located on outlet glaciers and c the ice-cap margins and inferred that such pixels probably contai a mixture of exposed rock, ice, and meltwater during the melt sea The presence of materials other than pure ice and snow within a p can, therefore, result in an LST greater than maximum temperatu pure ice and snow. To mitigate this effect, ice-covered pixels wit LST >0°C were reassigned a value of 0°C.

Commented [m24]: Rev. 2
RC 23: Page 5, lines 151-152 – The authors seem to generalize i that "uncertainties in the MOD11A2 LSTs arise mainly from clou contamination". Suggestion to reread relevant literature and prese accurately. Does the sentence refer to over snow only?
AR 23: This sentence referred to uncertainties in the trends deriv from the MOD11A2 data and not in the MOD11A2 data itself. T text has been revised for clarity.

Commented [m25]: Rev. 1
RC 11 Line 155: it should be stated that MOD11A2 Collection 6 were downloaded
AR 11: C6 added.

Commented [m26]: Rev. 2
RC 24: Page 6, line 159 – Is there a reference from precipitation records/data in QEI? i.e. what station, record or data is 400 mm/y derived from?
AR 24: The reference for the 400 mm/yr should be Braithwaite, 2005. This reference, included at the end of the following sentenc refers to both the temperature and precipitation ranges. Omitted reference now included.

To explore whether the~~re were~~ data contained any ~~other~~ spatial patterns that differed from the long-term (linear) trend, a Principal Components Analysis of the 16 year mean summer BSA record was performed using data from all pixels with mean summer BSA observations in every year (50% of pixels).

To investigate the spatial pattern of the relationship between surface temperature (LST) and albedo (BSA), linear correlations between the 16 year LST and BSA records were computed. The MCD43A3 C6 albedo data are produced daily whereas the MOD11A2 LST data are produced only every eight days. For this direct comparison between the LST and BSA data, eight day BSA averages were computed from the daily data for the same eight day periods as the MOD11A2 LST product, and resampled to a 1 km spatial resolution (nearest neighbour resampling). For each year, mean summer BSAs were computed from these eight day averages for all pixels having at least ~~seven~~ 7 of a possible ~~twelve~~ 12 observations, consistent with the computation of mean summer LST. ~~(Sect. 2.2).~~ The difference between the mean summer BSA values derived from these 8-day averages and those computed from the daily data (0.008) is within the uncertainty of MODIS reflectance products (0.05 for solar zenith angle <75°; Vermote et al., (2011)). Linear correlations between the 16 year BSA (eight day averaged) and LST records were then computed on a pixel-by-pixel basis for all pixels having LST and BSA observations in all years (~~80~~46% of all possible pixels).

To ensure that only data for glaciated surfaces were retained, all BSA and LST outputs used in this analysis were clipped to the Randolph Glacier Inventory v3.2 region 32 (Arctic Canada North) reference polygons (Arendt et al., ~~2013~~2012; Pfeffer et al., 2014). Surface elevations were obtained from the Canadian Digital Elevation Dataset (CDED) edition 3.0, scale 1:50 k, re-sampled to a 500 m resolution.

3 Results

3.1 Mean summer albedo

Annual maps of the mean summer clear-sky broadband shortwave black-sky MCD43A3 albedo for all glacier-covered surfaces in the QEI for the 2001-~~20~~16 period are presented in Fig~~.~~ ure 2. The QEI-wide mean summer BSA, averaged across all 16 years, was 0.550 ± 0.115 (mean ± 1 standard deviation; Table 1). The lowest QEI-wide mean summer BSA (0.539 ± 0.127) was recorded in 2011 while the highest (0.668 ± 0.089) was recorded in 2013 (Table 1).

In general, mean summer BSA is lower around the margins of the ice masses, where glacier ice is exposed in the summer, than it is in the higher elevation interior regions where snow or firn are exposed year-round (Fig. 2). During years when the QEI-wide mean summer BSA was low (e.g. 2011), we observed a broad zone of low albedo values (< 0.4) around the margins of the major ice masses (Fig. 2). Conversely, in years when the mean summer BSA was high (e.g. 2013), this zone was much less obvious. High data dropout at high elevations on Axel Heiberg Island, and over the summit of the Devon Ice Cap in 2014 and 2006 (Table S1), may have produced a negative albedo bias for these regions, since the albedo is typically greater at higher

Commented [m27]: Rev. 2
RC 8: Include references to Tables, methods as appropriate.
AR 8: Additional references to Tables, Figures, and methods hav been added throughout.

Commented [m28]: Rev. 2
RC 5: "Reorganization of content is advised toward readability. There are several cases where content is difficult to follow. Exam Results Section, 3.1 Suggestion to add sentences clarifying and further detailing results. As written, parts of the section are terse non-intuitive."
AR 5: Section 3.1 has been re-ordered and additional text has be added for readability.

Commented [m29]: Rev. 2
RC 25: Page 7, line 195 – Suggestion to include MCD43A3 for clarity and completeness.
AR 25: Mention of MCD43A3 included for clarity and complete as suggested.

elevations. Aggregating the 2001-16 average mean summer BSA into 50 m elevation bins, we observed a linear rate of BSA increase with elevation (0.0085 per 50 m elevation bin, $r^2 = 0.99$).

In addition to the mean summer (JJA) BSA, the monthly mean BSA values for June, July, and August, were also investigated (Sect. 2.3) (Table 2, Fig. S1-S3). July had the lowest 16-year monthly mean BSA (0.551 ± 0.131), followed closely by August (0.579 ± 0.127) (Table 2~~, Fig. S1-S3~~). In each year during the 2001-~~20~~16 period, the highest summer monthly BSA was always recorded in June while the lowest monthly BSA was recorded in either July or August. The lowest monthly mean BSA values for June and August were recorded in 2011, while the lowest~~; for~~ July~~, the lowest monthly~~ mean BSA occurred in 2012. The highest monthly mean BSA for both June and July occurred in 2013; for August, it occurred in 2003. ~~and may indicate early onset of snowfall that fall.~~

~~In general, mean summer BSA is lower around the margins of the ice masses than in the higher elevation interior regions (Fig. 2).~~ ~~Aggregating the 2001-2016 average mean summer BSA into 50 m elevation bins, we observed a linear rate of BSA increase with elevation (0.0085 per 50 m elevation bin, $r^2 = 0.99$).~~ ~~During years when the QEI-wide mean summer BSA was low (e.g. 2011), we observed a broad zone of low albedo values (< 0.4) around the margins of the major ice masses (Fig. 2). Conversely, in years when the mean summer BSA was high (e.g. 2013), this zone was much less obvious. High data dropout at high elevations on Axel Heiberg Island and over the summit of the Devon Ice Cap in 2014 and 2006 (Table S1), may have produced a negative albedo bias for these regions, since the albedo is typically greater at higher elevations.~~

3.2 Albedo anomalies

3.~~1~~2.1 Mean summer (JJA) BSA anomalies~~Albedo anomalies: 2001 to 2016~~

The mean summer BSA anomal~~y~~ies, relative to the 2001-16 mean, are presented in Figure 3 and Table 1. For consistency with the regression analysis (Sect. 3.3), BSA anomalies were only computed for pixels having mean summer BSA observations in 11 or more of the 16 years (Sect. 2.3). The period 2001-16 is characterised by a six~~-~~year period of positive BSA anomalies (2001-06) followed by a six year period of negative BSA anomalies (2007-12) (Table 1). ~~QEI-wide and regional BSA anomalies, relative to the 2001-2016 mean, were positive from 2001 to 2006 and negative from 2007 to 2012 (Table 1, Fig. 3).~~ Positive BSA anomalies were also observed in 2013 (+0.060) and 2014 (+0.015), while 2015 (-0.022) and 2016 (-0.005) saw a return to negative anomalies (Table 1). ~~For each region shown in Fig. 1, the most negative regionally-averaged BSA anomalies occurred in either 2001 or 2012, while the most positive regionally-averaged BSA anomalies occurred in either 2004 or 2013 (Table S2).~~ Negative BSA anomalies during 2007-~~20~~12, which indicate a larger absorbed fraction of incoming shortwave radiation relative to the 16-year mean, coincide, and are consistent with, positive summer air and glacier surface temperature anomalies in the QEI from 2007 to 2015 (Mortimer et al., 2016). Higher temperatures increase the rate of snow grain metamorphism which lowers the surface albedo (Wiscombe and Warren, 1980; Colbeck, 1982; Warren 1982), and a lower albedo increases the proportion of solar radiation absorbed at the ice-air interface, providing more energy for surface

Commented [m30]: Rev. 2
RC 7: For example, readers may appreciate a sentence stating tha addition to the JJA averages, monthly mean albedo was also calculated (Table 2, see Section 2.3).
AR 7: Section 3.1 (presented above) has been re-ordered to make easier to follow and a sentence (Line 209) regarding the monthly BSA mean albedo with reference to the appropriate Table, Figure and methods section, has been added.

Commented [m31]: Rev. 2
RC 6: Lines 196-197 Why does Table 1 2001-2016 average diffe from manuscript stated average (i.e. Table 1 states 0.599, manusc states 0.550)?
AR 6: The value of 0.599 in Table 1 refers to the mean summer (BSA. The value of 0.551 on line 196-107 refers to the July mean BSA which is 0.551 ± 0.0131 and is presented in Table 2.

Commented [m32]: Rev. 2
RC 10: Two specific areas of speculation are: (1) Results Section 3.1, line 203, 'may indicate early onset of snowfall that fall' and Results Section 3.2, lines 290-292 snowfall patterns may be chan in QEI). Quantified data based statements are preferred over speculation where possible.
AC 10: Again, while we agree that quantitative statements are preferred over speculation the absence of in-situ precipitation lim our ability to do this. The specific areas of concern noted in RC 1 have been removed from the manuscript.

warming and melt. This positive feedback mechanism may have contributed to the tripling of glacier mass loss from this region between 2004-06 and 2007-09 (Gardner et al., 2011).

There was no year in which the BSA anomalies for all glaciated pixels were either all positive or all negative. The lowest amount of spatial variability in mean summer BSA anomalies (Fig. 3) was observed in years when the QEI-wide mean summer BSA anomaly was either extremely positive (2004 and 2013) or extremely negative (2011 and 2012) (~~Fig. 3~~Table 1). In 2004 and 2013 (large positive QEI-wide BSA anomalies), large positive BSA anomalies (> 0.1) were observed ~~mainly~~ at lower elevations around the margins of the ice masses, while BSA anomalies were near zero at higher elevations in the interiors of the ice masses (Fig. 3). In 2011 and 2012 (large negative QEI-wide BSA anomalies), a similar spatial pattern, but with anomalies of opposite~~, sign, spatial pattern~~ was observed~~, with large negative BSA anomalies occurring at low elevations; expect on the Devon Ice Cap in 2012 when BSA anomalies over most of the ice cap were near zero (> -0.0125).~~

T~~t~~he largest amount of spatial variability in the mean summer BSA occurred in years when the QEI-wide BSA anomaly was near zero (between ~-0.0048 and +0.0030; Table 1). In 2005, 2006, and 2016, BSA anomalies in a region that includes the eastern half of the Devon Ice Cap, the majority of the Manson Icefield, and the southernmost portion of the Prince of Wales Icefield were often opposite to those observed in the rest of the QEI (Fig. 3). These regions are in close proximity to open water sources in Baffin Bay (Fig. 1) which is largest moisture source for the QEI (Koerner, 1977). Variability in the extent of open water in the QEI's interisland channels has previously been correlated with the variability in summer temperatures (Koerner, 1977) and the 500 hPa geopotential height anomalies in the QEI (Bezeau et al., 2015). Nearby open water sources may serve to moderate the surface albedo variability in this eastern maritime region through more frequent and/or persistent snowfall and riming events in warm summers when the open water extent is large (Koerner, 1977; 1979; Alt, 1978). ~~In years when the QEI-wide BSA anomaly was near zero (between ~-0.0048 and +0.0030; Table 1), BSA anomalies were of opposite sign to those in the rest of the QEI in a region that includes the eastern half of the Devon Ice Cap, the majority of the Manson Icefield, and the southernmost portion of the Prince of Wales Icefield (Fig. 3). In 2005 and 2006 when the QEI-wide BSA anomalies were small and positive (0.0035 and 0.0030, respectively), BSA anomalies in this region were negative. Conversely, in 2016 when the QEI-wide BSA anomaly was small and negative (-0.0048), large negative BSA anomalies were observed in this region while only weak negative, or even positive, BSA anomalies occurred elsewhere. This eastern maritime region is located close to open water sources in Baffin Bay (Fig. 1). These areas may moderate surface albedo variability through more frequent and/or persistent snowfall and riming events in warm summers when the open water extent is large (Koerner, 1977; 1979; Alt, 1978).~~

In 2005 and 2006 (years when the mean summer QEI-wide BSA anomaly was near zero and there was a large amount of spatial variability in the mean summer BSA), ~~large~~ BSA anomalies on the western-most part of Axel Heiberg Island (< -0.05; Fig. 3) were double the magnitude of the QEI-wide BSA anomaly (Table 1) and were of the same sign. A similar feature (large anomaly values of the same sign as the QEI-wide anomaly) was also observed in the LST anomaly record in 2005 (Fig. S7). ~~In years when BSA anomalies in maritime regions of the southeastern QEI were opposite to those in the rest of the QEI, BSA anomalies on the western-most part of Axel Heiberg Island tended to be large (< -0.05; Fig. 3) though of the same sign as the~~

~~QEI-wide BSA anomaly (Table 1).~~ Examination of the 500 hPa geopotential height anomalies for 2001-2016 in NCEP/NCAR reanalysis R1 data (Kalnay et al., 1996; https://www.esrl.noaa.gov/psd) ~~reveals~~ shows that in years when the mean summer QEI-wide BSA anomaly was strongly negative (e.g. 2001-~~20~~04) (or positive (e.g. 2007-~~20~~12)) a persistent ridge (trough) was centred over the north and west of the QEI (which includes Axel Heiberg Island) (Fig. 4). These circulation features are likely responsible for the strong negative BSA anomalies observed over Axel Heiberg Island because~~,~~ c~~C~~lear sky conditions that accompany anticyclonic circulation increase the proportion of incoming shortwave radiation received at the air-ice interface, providing more energy for melt, and driving albedo decline.

~~Finally, when the QEI-wide BSA anomaly was small and positive (<0.03, e.g. 2001 and 2003), BSA anomalies on either side of the north-south trending mountain ranges of eastern Ellesmere and Devon Islands were typically of opposite sign. For example, in 2001, positive BSA anomalies occurred on Devon Ice Cap (southeast QEI) and on the eastern side of the north-south trending mountain range of eastern Ellesmere Island, while negative BSA anomalies occurred in the north and west of the QEI (Fig. 3). We note, however, that there were also instances of instances of positive BSA anomalies at higher elevations in the interior regions of the ice masses on Axel Heiberg Island and northwest Ellesmere Island. In 2003, negative BSA anomalies dominate the south and east of the QEI while BSA anomalies were positive in the northwest of Ellesmere Island and generally negative on Axel Heiberg Island (western QEI). This southeast-northwest spatial pattern is similar to the pattern of LST change described by Mortimer et al. (2016) where LST change was greatest in the north and west of the QEI.~~

3.2.2 Summer monthly BSA anomalies

In addition to the mean summer (JJA) BSA anomalies, the mean June, July, and August BSA anomalies were also examined (Fig. S4-S6) (Sect. 2.3). ~~The spatial pattern of BSA anomalies also varies from month to month (Fig. S4-S6).~~ T~~t~~he sign of the mean July BSA ~~QEI-wide BSA~~ anomaly (Table 2) was always ~~the same~~consistent ~~as~~with that of the mean summer (JJA) ~~QEI-wide~~ BSA anomaly (Table 1) ~~2, Fig. S5).~~ In contrast, the sign of the mean June and August QEI-wide BSA anomaly was often opposite to that of the mean summer BSA anomaly. In June, negative QEI-wide BSA anomalies occurred in 2002 and 2005 when the mean summer QEI-wide BSA anomaly was positive, while positive QEI-wide BSA anomalies occurred in 2007 and 2009 when the mean summer BSA anomaly was negative. Negative QEI-wide BSA anomalies occurred in August 2005 and 2006, when the QEI-wide mean summer anomaly was positive; positive BSA anomalies occurred in August 2010, 2015 and 2016, when the QEI-wide mean summer anomaly was negative. ~~June BSA anomalies were generally characterized by a southeast-northwest spatial pattern.~~

There are also distinct differences in the large-scale spatial patterns of the BSA anomaly between months. In years with strong negative (positive) QEI-wide June BSA anomalies, most of the ice-covered pixels also ~~QEI~~ had negative (positive) anomalies, in this month (Fig. S4). ~~and the largest negative (positive) anomalies were observed at low elevations around the margins of the ice masses in the continental interior (Fig. S4).~~ In contrast, i~~I~~n years with weak negative QEI-wide June BSA anomalies

(e.g. 2002), positive (June BSA) anomalies occurred in the southeast while, negative BSA anomalies occurred in the west and northwest (Fig. 4). The opposite scenario occurred in years with weak positive QEI-wide June BSA anomalies (e.g. 2003). In July (Fig. S5), (the month with the lowest QEI-wide BSA, Table 2), when the mean monthly BSA was typically lowest, BSA anomalies were typically both large (-0.0805 to +0.0843) and less spatially variable than in either June or August (Fig. S4 and S6). However, in some years (e.g. 2005) July BSA anomalies in the southeast maritime region that includes the eastern part of the Devon iIce capC, Manson Icefield and the south-easternmost part of the Prince of Wales Icefield were opposite in sign to those over the rest of the QEI. Nearby open water sources may have moderated the BSA in this region (Sect. 3.2.1). , and the sign of the July QEI-wide BSA anomaly was always the same as that of the mean summer (JJA) QEI-wide BSA anomaly (Table 2, Fig. S5).

Mean August BSA anomalies displayed higher spatial variability than July anomalies, but were typically of similar magnitude (-0.0657 to +0.0836, Table 2). Unlike the June BSA anomalies (Fig. S4), which are characterized by a northwest-southeast spatial pattern, spatial variations in the August BSA anomaly are more local (zonal) in nature (Fig. S6). Cyclonic circulation is much more prevalent over the QEI in August than in June and July (Alt, 1987; Gascon et al., 2013). The zonal nature of the August BSA anomaly likely reflects localized snowfall events related to the passage of individual low-pressure systems, associated with cyclonic circulation conditions. These snowfalls would temporarily raise the surface albedo in affected regions.

3.2 3 Albedo change: 2001–162001 to 2016

3.3.1 Mean summer BSA change

To determine whether there was a measurable change in the summer surface albedo over the period 2001-16 we performed a linear regression. Regressions were performed on a pixel-by-pixel basis for all pixels having mean summer BSA observations in at least 11 of the 16 years of observation (Sect. 2.3). The QEI-wide rate of change was taken as the average for these pixels. Between 2001 and 2016 the mean summer (JJA) QEI-wide BSA decreased at a rate of 0.0029 ± 0.0025 yr^{-1} (Table 23, Fig. 54a). As More than 95% of pixels experienced a non-negligible (> |0.001| yr^{-1}, Sect. 2.3) decrease in summer BSA and the total BSA change (-0.046) exceeds the MODIS sensor capabilities (2% in absolute reflectance units for the reflective solar bands (0.41-2.2 µm) (Justice et al., 1998) (Sect. 2.1), suggesting that the mean summer BSA did decline somewhat during this 16-year period. Although the measured change in the QEI-wide mean summer BSA (average correlation coefficient of all pixels) (r = 0.31, p = 0.24) was not statistically significant (r = 0.31, p = 0.24), BSA declines that were significant at the $p \leq 0.05$ significance level were observed at the pixel level on all ice masses (Fig. 6a). The BSA change reported here is comparable to, although slightly larger, than, that identified for the Greenland Ice Sheet's wet snow zone over the same time period (2001-2016) using similar data (-0.00254 decadeyr^{-1} for MCD43A3 Band 4 (545 – 565 µm)) (Casey et al., 2017). Furthermore, the measured albedo decline exceeds the detection limit of the MODIS C6 calibration accuracy (0.01 decade^{-1}; Lyapustin et al. (2014)), suggesting that BSA did decline somewhat during this 16-year period. There was a larger (but still not significant) decrease in the QEI-wide mean July BSA (-0.0050 ± 0.0031 yr^{-1}, r = 0.38, p = 0.15), while no QEI-wide change was observed

Commented [m33]: Rev. 2
RC 26: Page 9, line 272 – Note that it is not only the calibration accuracy that limits the capability to measure trends, but also the sensor design. Please add reference to sensor capabilities (e.g. Ju et al., 1998, doi: 10.1109/36.701075 and/or similar on MODIS instrument design and post-launch capabilities, see https://mcst.gsfc.nasa.gov/publications?f%5Btype%5D=102).
AR 26: Sentence revised for accuracy in both the methods and re sections. Additional references to the appropriate methods sectio and literature have been included.

~~in either June or August (Table 3, Fig. 5), suggesting that the bulk of the mean summer BSA decline occurred in the month of July. In July, > 93% of pixels exhibited a detectable decrease in BSA and 24% of the measured BSA declines were significant at the p < 0.05 level. The BSA change reported here is comparable to, although slightly larger, than that identified for the Greenland Ice Sheet's wet snow zone over the same time period (2001-2016) using similar data (-0.0254 decade^{-1} for MCD43A3 Band 4 (545 – 565 μm)) (Casey et al., 2017).~~

Between 2001 and 2016, the area-averaged mean summer (JJA) incoming solar radiation over ice covered surfaces in the QEI, computed from daily means of NCEP/NCAR R1 Reanalysis data (Kalnay et al., 1996) (http://www.esrl.noaa.gov/psd/data/gridded/), ranged from 346 W m^{-2} (clear-sky downward solar flux) to 299 W m^{-2} (all-sky downward solar flux). Assuming the solar radiation received at the surface was constant over the ~~16~~ 16-year period, our measured BSA reduction (-0.0029 yr^{-1}) translates to a total increase in area-averaged absorbed solar radiation of between 1.1 and 1.4 MJ over the 16 year period. For a surface already at the melting point, this would equate~~s~~ to an increase in (area-averaged) summer melt of between 0.38 and 0.44 m w.e. (Cuffey and Paterson, 2010 Table 5.1).

Spatially, large reductions in the mean summer BSA (< -0.005 yr^{-1}) occurred at lower elevations around the margins of the ice masses (where the mean summer BSA is lowest), especially on Axel Heiberg Island, northern Manson Icefield, and on the continental (western) side of the ice masses on Ellesmere Island (Fig. 5a). Many of these BSA declines were significant at the $p \leq 0.05$ level (Fig. 6a). Statistically significant BSA declines (~ -0.00357 yr^{-1}, $p \leq 0.05$) also occurred in the interior of the Manson Icefield and on the southern half of the Devon Ice Cap (Fig. 5a, 6a). Although BSA declines tended to be larger at lower elevations, slight BSA increases (> 0.001 yr^{-1}, not statistically significant) ~~Detectable (although not statistically significant) BSA increases (> 0.001 yr^{-1})~~ were observed along the lower portions of outlet glaciers (Fig. 6a). ~~and may point to an increased occurrence of summer snowfall events and/or a later removal of the previous year's snowpack (either from higher fall/winter snow accumulation and/or later melt onset).~~ Many of these glaciers are close to open water sources where ~~In addition, in areas close to the oceans,~~ coastal fog may play a role in reducing summer melt, thereby suppressing albedo declines ~~over the lower portions of outlet glaciers~~ (Alt, 1987). ~~These variations likely contributed to the low correlation coefficients along the lower reaches of many outlet glaciers.~~ No ~~detectable~~ measurable change~~s~~ in mean summer BSA ~~was~~ were observed over the high elevation (> ~1500 m a.s.l.; > ~1200 m a.s.l for Sydkap Ice Cap) interior regions of the Devon Ice Cap, Sydkap Ice Cap, Agassiz Ice Cap, Prince of Wales Icefield, or northern Ellesmere Island ice caps, even though strong increases in LST were observed in these locations between 2000 and ~~2015~~ 2016 (Fig. 7). ~~(Mortimer et al., 2016). Figure 6a also shows a large cluster of pixels with significant declines in mean summer BSA (~ -0.00357 yr^{-1}, $p \leq 0.05$) in the interior of the Devon Ice Cap.~~

~~The spatial pattern of BSA change in July (the month when BSA decrease was largest) is similar to the spatial pattern of mean summer BSA, with the largest BSA declines occurring at lower elevations (Fig. 5c). In July, BSA trends at the $p \leq 0.05$ significance level (Fig. 6c) coincide, in general, with those locations having the largest BSA declines (< -0.0075 yr^{-1}). Statistically significant BSA declines occurred in the continental interiors of all the ice masses on Ellesmere Island, as well as~~

~~on the northern half of Axel Heiberg Island, the southern Prince of Wales Icefield, northern Manson Ice Cap, and southwest Devon Ice Cap.~~

~~Although no significant QEI-wide BSA change was observed in either June (-0.0017 ± 0.0024 yr^{-1}) or August (-0.0022 ± 0.0036 yr^{-1}), owing to the large amount of spatial variability in the sign and magnitude of BSA change in these months, local areas of consistent BSA change are observed. In June, increases in BSA occurred on the eastern portions of Prince of Wales Icefield and Agassiz Ice Cap, while weak-to-moderate BSA declines (≥~ -0.005 yr^{-1}) occurred elsewhere. We note, however, that only 10% of pixels had June mean BSA trends significant at the p ≤ 0.05 level. These pixels are mainly found on the southwest parts of the Devon and Agassiz Ice Caps and in northwest Ellesmere Island (Fig. 6b).~~

~~In August, large and statistically significant BSA declines (< -0.00625 yr^{-1}, p ≤ 0.05) occurred on the eastern Devon Ice Cap, Manson Icefield, and southeast Prince of Wales Icefield (Fig. 6d). Moderate August mean BSA declines (< -0.005 yr^{-1}, p ≤ 0.05) occurred on the northern half of northwest Ellesmere Island. August mean BSA increased on the summits of Devon Ice Cap and Sydkap Ice Cap, in the western part of Prince of Wales Icefield, in some eastern and southerly sections of the Agassiz Ice Cap, and on some outlet glaciers in northwest Ellesmere Island and Axel Heiberg Island. These increases, however, were not statistically significant.~~

3.3.2 Summer monthly BSA change

~~**3.3.2 Summer monthly BSA change: 2001 to 2016**~~

In addition to the mean summer BSA change, trends in the mean monthly (June, July, and August) BSA were also investigated (Sect. 2.3). Maps of the mean monthly BSA change, presented in Figures 5b-d, illustrate differences in the spatial patterns of BSA change for each summer month. There was a large~~r~~ (but ~~still~~ not significant at the ~~P~~p < 0.05 level) decrease in the QEI-wide mean July BSA (-0.0050 ± 0.0031 yr^{-1}, r = 0.38, p = 0.15), ~~while~~but no QEI-wide change was observed in either June or August (Table 3~~, Fig. 5~~). This~~,~~ suggest~~s~~ing that the bulk of the mean summer (JA) BSA decline occurred in the month of July. In July, > 93% of pixels exhibited a ~~detectable~~non-negligible decrease in BSA (Fig. 5c), and 24% of the measured (July) BSA declines were significant at the p < 0.05 level. The spatial pattern of July BSA change ~~in July~~(Fig. 5c) ~~(the month when BSA decrease was largest)~~ is similar to that ~~the spatial pattern~~ of mean summer BSA change (Fig. 5a), with the largest BSA declines occurring at lower elevations ~~(Fig. 5c).~~ In ~~this month~~July, statistically significant (p < 0.05) BSA ~~declines~~decreases occurred in the climatically continental interior ~~s~~regions of all the ice masses on northern Ellesmere Island, ~~as well as~~ on the northern half of Axel Heiberg Island, the southern Prince of Wales Icefield, northern Manson ~~Ice Cap~~Icefield, and the southwest Devon Ice Cap (Fig. 5c, 6c). ~~In July, BSA trends at the p ≤ 0.05 significance level (Fig. 6c) coincide, in general, with those locations having the largest BSA declines (< -0.0075 yr^{-1}). Statistically significant BSA declines occurred in the continental interiors of all the ice masses on Ellesmere Island, as well as on the northern half of Axel Heiberg Island, the southern Prince of Wales Icefield, northern Manson Ice Cap, and southwest Devon Ice Cap.~~

Although ~~no~~there was no measurable change ~~significant~~in the QEI-wide BSA ~~change was observed~~ in either June (-0.0017 ± 0.0024 yr^{-1}) or August (-0.0022 ± 0.0036 yr^{-1}), owing to the large amount of spatial variability in the sign and magnitude of BSA changes in these months, ~~local~~notable clusters ~~areas~~ of consistent BSA change are observed (Fig. 5b, 5d). In June, increases in BSA occurred on the eastern portions of Prince of Wales Icefield and Agassiz Ice Cap, while weak-to-moderate BSA declines (>~ -0.005 yr^{-1}) occurred elsewhere (Fig. 5b). ~~We note, however, that~~In June, only 10% of pixels had ~~June mean~~ BSA trends that were significant at the $p \leq 0.05$ level.~~;~~. ~~T~~tThese pixels are found mainly ~~found~~ on the southwestern parts of the Devon and Agassiz Ice Caps, and in northwest Ellesmere Island (Fig. 6b).

In August, large and statistically significant BSA ~~declines~~decreases (< -0.00625 yr^{-1}, $p \leq 0.05$) occurred on the eastern Devon Ice Cap, Manson Icefield, and southeast Prince of Wales Icefield (Fig. 5d, 6d). Moderate declines in August mean BSA ~~declines~~ (< -0.005 yr^{-1}, $p \leq 0.05$) occurred on the icefields in the northern half of northwest Ellesmere Island. The mean August ~~mean~~ BSA increased on the summits of the Devon ~~Ice Cap~~ and Sydkap Ice Caps, in the western part of the Prince of Wales Icefield, in some eastern and southerly sections of the Agassiz Ice Cap, and on some outlet glaciers in northwest Ellesmere Island and Axel Heiberg Island (Fig. 5d). However, t~~T~~hese increases~~, however,~~ were not statistically significant (Fig. 6d).

3.~~3~~ 4 Principal ~~components~~ Components ~~analysis~~Analysis

To explore whether there are any other spatial patterns in the 16-year mean summer BSA record that differ from the long-term (linear) trend, we performed a Principal Components Analysis of the BSA record (Sect. 2.3). The first and second Principal Components (Fig. ~~7~~8) explain 65% and 12% of the variance in the mean summer BSA record, respectively. The spatial pattern of the First Principal Component (PC1) scores (Fig. ~~7a~~8a) is generally consistent with the spatial patterns of summer (JJA, Fig. 5a) and July (Fig. 5c) mean BSA change described previously (Sect. 3.2~~), Fig. 5a,c)~~. PC1 scores are strongly negative (< -0.005) on western Axel Heiberg Island (large BSA declines), and weakly negative (> -0.001) or even positive at high elevations in the interiors of the ice masses where there was no ~~detectable~~ change in mean summer BSA ~~was observed~~. Moderately negative (~ -0.002) component scores occur on the western (continental) side of eastern Ellesmere Island's ice masses as well as over much of Manson Icefield and the southeast portion of Prince of Wales Icefield, where large decreases were observed in both summer (JJA) and the July BSA.

For PC1, the highest Empirical Orthogonal Functions (EOFs) (32.8 and 25.9) correspond to the years with the lowest mean summer BSA (2011 and 2012) (Fig. ~~8~~9). The lowest EOFs (-31.7 and -24.6) correspond to the years with the highest mean summer BSA (2013 and 2004). In addition, the departure from zero is much larger for the minimum component scores than for the maximum component scores (Fig. ~~7a~~8a), suggesting that both positive and negative BSA anomalies are likely caused by forcings with the same spatial pattern, albeit with the opposite sign. Investigating possible relationships between surface albedo and known large-scale patterns of atmospheric variability (Arctic Oscillation, Pacific North American Pattern, North Atlantic Oscillation), we found the EOFs for PC1 to be well (negatively) correlated with the mean summer North Atlantic

Commented [m34]: Rev. 1
RC 13 Line 319: I think sections 3.3 and 4.1 could be shortened made to be more concise
AR 13 Sections 3.3 and 4.1 have been shortened. Repetition in sections 3.3 and 4.1 has been removed. Section 4.1 and 4.2 have merged.

Oscillation (NAO) index (r = -0.84, p < 0.001, Fig. ~~8~~9), derived by averaging the June-August monthly mean NAO indices for 2001 to 2016 (http:www.cpc.ncep.noaa.gov). This is consistent with the finding of Mortimer et al. (2016) that there was a good agreement between the mean summer LST record and the NAO index in the QEI over the 2000-15 period. ~~From 2007-2012, when both the NAO index and BSA anomalies were negative (Fig. 8),~~ the frequency of anticyclonic circulation over the QEI in summer doubled relative to the 1948-2012 mean (Bezeau et al., 2015). ~~Clear-sky conditions that accompany anticyclonic circulation increase the proportion of incoming shortwave radiation received at the air-ice interface, providing more energy for melt and driving albedo decline.~~

~~The spatial pattern of the second Principal Component (PC2) scores (Fig. 7b) resembles that of the August BSA change (Fig. 5d). Large negative component scores (< -0.004) were observed on eastern Devon Ice Cap and Manson Icefield, where large August BSA declines (< -0.0075 yr^{-1}) occurred. Positive component scores were observed in the in southwest Axel Heiberg Island and at lower elevations on northern Ellesmere Island's southwestern ice caps, where the mean August BSA increased (Fig. 5d).~~

The second Principal Component (PC2) had the largest EOFs of any component in 2006, 2010, and 2016. In these years, ~~the mean August BSA anomaly in these regions was of opposite sign to that of the mean summer (JJA) anomaly, and~~ there was poor correspondence between the PC1 EOFs and the JJA NAO index (Fig. ~~8~~9). The spatial pattern of the second Principal Component (PC2) scores (Fig. ~~7~~8b) resembles that of the August BSA change (Fig. 5d). Large negative ~~component~~PC2 scores (< -0.004) were observed on eastern Devon Ice Cap and Manson Icefield, where large August BSA declines (< -0.0075 yr^{-1}) occurred. Positive ~~component~~PC2 scores (Fig. 8b) were observed in ~~the in~~ southwest Axel Heiberg Island and at lower elevations on northern Ellesmere Island's southwestern ice caps, where the mean August BSA increased (Fig. 5d). Unlike PC1, there were no significant correlations between the EOFs of PC2 and known large-scale patterns of atmospheric variability.

~~Examination of the cumulative mass change record for the QEI from the Gravity Recovery and Climate Experiment (GRACE; Wolken et al. (2016), extended to 2016) shows that in the same years (2006, 2010, 2016), once the annual minimum glacier mass was reached, there was a prolonged period of constant but low mass (i.e. no melt or snowfall) before fall/winter accumulation began (inferred from an increase in mass). In other years, there was a sharp transition from the local end-of-summer mass minimum to the period of seasonally increasing mass. There is also good correspondence between the spatial pattern of PC2 scores and the spatial pattern of snow accumulation and $\delta^{18}O$ values that was inferred for the 1962-1974 period from surface snow samples and shallow firn cores collected in spring 1974 (Koerner, 1979). Areas having large negative PC2 component scores (< -0.004) were characterized by relatively high accumulation rates (Fig. 2 and 3 in Koerner (1979)) and snow that is isotopically warm (Fig. 7 in Koerner (1979)). Areas with positive PC2 component scores had lower snow accumulation rates. The correspondence between the pattern of PC2 component scores (Fig. 6b) to previously reported snow accumulation patterns over the QEI, and the spatial pattern of change in the August mean BSA (Fig. 4d), suggests that anomalously low snow accumulation in August may have influenced the mean summer BSA in those years when PC2 had the largest EOFs (e.g. 2006, 2010, and 2016).~~

3.5 Comparison with the mean summer LST

Owing to the positive feedback between albedo and surface temperature we would expect to observe strong increases in surface temperature where albedo declines were large. To investigate the relationship between temperature and albedo over the QEI the 16 year mean summer LST record was compared with the 16 year mean summer BSA record (Sect. 2.3). Due to the 8-day averaging period of the MOD11A2 data used here, the mean monthly BSA were not included in this comparison (Sect. 2.3). Between 2001 and 2016, the mean summer LST (-3.0 ± 1.8°C) increased at a rate of 0.049 ± 0.038 °C yr^{-1} (Table 3). LST increases (Fig. 7b) were greatest at higher elevations where the mean summer LST (Fig. 7a) is lower~~;~~. ~~I~~in contrast, BSA decreases (Fig. 5a) were largest at lower elevations where the mean summer BSA was lowest (Fig. 2). This observation may be explained by the fact that, at lower elevations where the mean summer LST regularly reached the melting point, there was less potential for warming than at higher elevations (Mortimer et al., 2016).

As expected, the 16-year QEI-wide LST record was negatively correlated (r = -0.86) with the 16 year QEI-wide BSA record. This negative correlation points to a positive ice-albedo feedback that would enhance rates of glacier mass loss from the QEI. Spatially, correlations (derived from linear correlations between the 16 year LST and BSA records for each pixel (Sect. 2.3)) were strongly negative in the north and west ~~to~~of the QEI (Fig. 10). Weaker (negative) correlations (Fig. 10) occurred on the southwest Devon Ice Cap~~,~~ and Manson Icefield where LST decreased (Fig. 7b) and BSA increased (Fig. 5a). In these regions, where the mean summer LST is high, the weak correlations between LST and BSA may reflect the fact that the albedo continues to decline once the surface temperature has reached the melting point. We note, however, that the large amount of missing data limits our ability to discern broad spatial patterns of the relationship between LST and BSA in the QEI.

4 Discussion

~~4.1 Summer and monthly BSA~~

Between 2001 and 2016 ~~Our results show that~~ the bulk of the measured mean summer BSA declines in the ~~mean summer~~ QEI ~~albedo~~ occurred in July (Sect. 3.2)~~., which~~This finding is consistent with previous work (e.g. Alt, 1987; Gardner and Sharp, 2007) that found variability in July near-surface air temperatures to be the primary influence on inter-annual variability in annual QEI mass balance. Variability in July air temperatures has, in turn, been associated with ~~the~~ variations in the strength, position, and geometry of the July circumpolar vortex (Gardner and Sharp, 2007). Extreme high melt years in the QEI are associated with the intrusion of a steep ridge at all levels in the troposphere and the absence of the North American trough, making the QEI thermally homogeneous with continental North America (Alt, 1987). Between 2001 and 2016, in warm years with low (e.g. 2007-2012) (high (e.g. 2001-2004)) albedos, there was a persistent ridge (trough) in the 500 hPa geopotential height surface centered over the north and west of the QEI (Fig. 4; Sect. 3.1.1;). This configuration appears to be tied to the increased warming and albedo declines observed in the central western part of the QEI from 2007 to 2012. For example, strong

warming and albedo declines over Axel Heiberg Island and north-central Ellesmere Island coincided with a ridge of high pressure centered over the north and west of the QEI that was often observed in years when the NAO index was negative (Fig. 9).

Differences in the s~~S~~patial ~~variations~~patterns of ~~in~~ the monthly BSA change (Fig. 5b–d) ~~also~~ reflect the ~~different~~dominant atmospheric circulation patterns that occur over the QEI during the ~~course of~~ the summer months. In the QEI, anticyclonic circulation tends to dominate in the months of June and July, while cyclonic circulation often occurs in August (Alt, 1987; Gascon et al., 2013).

In ~~In contrast to~~ June and July, ~~when~~ the largest BSA declines occurred in the ~~west~~climatically continental interiors of the ice masses on Ellesmere and Devon Islands, as well as on Axel Heiberg Island (Fig. 5). In these months, the mountains on eastern Ellesmere and Devon Islands act as a barrier to moisture transport from the east limiting (solid) precipitation (which can temporarily raise the surface albedo) on the western (lee) side of the eastern ice masses (Koerner, 1979). Adiabatic heating of descending air masses on the western (lee) side of the eastern ice masses results in warm dry air which promotes warming, melting, and enhance~~d~~d albedo declines ~~of the QEI, BSA declines in August were largest at low elevations in the maritime regions of eastern Devon Ice Cap, Manson Icefield, and the southwestern Prince of Wales Icefield (Fig. 5).~~ In contrast, in August, when ~~As mentioned in Section 3.2.1, August weather in the QEI tends to be dominated by~~ cyclonic circulation is commont (Sect. 3.2.1) (Alt, 1987; Gascon et al., 2013) BSA declines were largest at low elevations in the maritime regions of eastern Devon Ice Cap, Manson Icefield, and the southwestern Prince of Wales Icefield (Fig. 5d). ~~,~~ Low pressure systems which track from the southwest to the north and northeast are common in August, and they advect warm moist air into the Arctic from the south (Alt, 1987; Gascon et al., 2013). In the eastern QEI, orographic uplift of air masses tracking from the southwest, and subsequent adiabatic heating of these air masses when they descend on the eastern sides of ice masses, would bring warm dry air to the eastern (lee) side of the mountains in the eastern QEI, promoting both warming and albedo decline in these regions in August.

During the 2001-16 period, the mean summer QEI-wide BSA record was strongly tied to the summer NAO index (Sect. 2.4). ~~Inter-annual variations in the QEI mean summer LST anomalies have previously been linked to variations in the NAO index (Mortimer et al., 2016). Here we find that the 16-year record of summer BSA is also strongly tied to the summer NAO index (Sect. 3.3). In years with strong negative (positive) BSA anomalies and positive (negative) LST anomalies (e.g. positive: 2007-2012, negative: ; 2013; see Mortimer et al. (2016)) the NAO index was negative (positive). During the 2007-2012 period when the NAO index was negative (Fig. 8), there was an increase in the frequency of A~~anticyclonic circulation~~, compared to the 1948-2012 mean (Bezeau et al., 2015). Similarly, over the Greenland Ice Sheet, strong anticyclonic ridging, associated with clear skies and the advection of warm air from the south~~, was found shown to co-vary with the NAO index over the Greenland Ice Sheet, immediately to the east of the QEI, over the period since ~2001 (Rajewicz and Marshall, 2014). On the Greenland Ice Sheet, clear sky conditions and the advection of warm air from the south which accompany anticyclonic ridging (Rajewicz and Marshall, 2014), similar to that observed in the QEI in June and July (Alt, 1987; Gascon et al., 2013; Bezeau et al., 2015). These conditions were found to enhance the strength of the ice-albedo feedback on the Greenland Ice Sheet during

Commented [m35]: Rev. 2
RC 27: Page 12, lines 365-366, Suggestion to reword sentence, avoiding use of "positive (negative)" words side by side.
AR 27: We find this to be an efficient way of writing. No change made.

~~from~~between 2009~~–~~ and 2011, which ~~resulting~~ resulted in higher rates of melt and glacier mass loss (Box et al., 2012). Although a similar phenomenon is likely to have occurred in the QEI, we find that in some years (2006, 2010, 2016) there was poor correspondence between the mean summer BSA record and the NAO index (Fig. ~~8~~9), suggesting that an additional forcing may be influencing the spatial and temporal variability of glacier surface albedo in the QEI.

~~In 2006, 2010, and 2016, the spatial pattern of BSA anomalies (Fig. 3) closely resembles that of the mean August BSA change (Fig. 5d), which, in turn, closely resembles the spatial pattern of PC2 component scores (Fig. 8b)~~

~~There is also good correspondence between the spatial pattern of PC2 scores and~~ T~~t~~he spatial pattern of snow accumulation (Fig. 2 and 3 in Koerner 1979) and $\partial^{18}O$ values(Fig. 7 in Koerner 1979) ~~that was~~were inferred by Koerner (1979) for the 1962-~~1974~~3 period from surface snow samples and shallow firn cores collected in spring 1974. ~~(Koerner, 1979).~~ These spatial patterns (of snow accumulation and $\partial^{18}O$) closely resemble the spatial pattern of PC2 scores (Fig. 8b). Specifically, a~~A~~reas having large negative PC2 component scores (< -0.002, Fig. 8b4) of the 16-year mean summer BSA record (Sect. 3.4) were characterized by relatively high accumulation rates (Fig. 2 and 3 in Koerner (1979)) and snow that is isotopically warm (Fig. 7 in Koerner (1979)).~~ while a~~A~~reas with positive PC2 component scores had lower snow accumulation rates. This similarity points to a possible role of precipitation in affecting the mean summer BSA in some years. ~~The correspondence between the pattern of PC2 component scores (Fig. 6~~8b~~), to previously reported snow accumulation patterns over the QEI, and and the spatial pattern of the mean August change in the August mean BSA change (Fig. 4~~5~~d), suggests that anomalously low snow accumulation in August may have influenced the mean summer BSA in those years when PC2 had the largest EOFs (e.g. 2006, 2010, and 2016).~~ To investigate the relationship between the albedo record and variability in precipitation we ~~E~~examin~~ation~~ed ~~of~~ the cumulative mass change record for the QEI from the Gravity Recovery and Climate Experiment (GRACE; Wolken et al. (2016), extended to 2016 (B. Wouters, personal communication, 2017)). The record shows that in 2006, 2010, 2016 (the years when PC2 of the 16-year mean summer BSA record had the largest EOFs of any Principal Component, Sect. 3.4), once the annual minimum glacier mass was reached, there ~~was~~has been ~~was~~ a prolonged period of constant ~~but~~ low mass (i.e. no melt or snowfall) before fall/winter accumulation began (inferred from an increase in mass). In other years, there was a sharp transition from the local end-of-summer mass minimum to the period of seasonally increasing mass.

~~. In these years, delayed snowfall onset and limited melt in August were inferred from the GRACE mass change record.~~ This could indicate that in some years during the 2001-2016 period, variability in August snowfall, ~~in addition to that tied to the NAO,~~ may have influenced the mean summer BSA.

~~Spatial variations in the monthly BSA reflect the different atmospheric circulation patterns that occur over the QEI during the course of the summer. In the QEI, anticyclonic circulation tends to dominate in the months of June and July, while cyclonic circulation often occurs in August (Alt, 1987; Gascon et al., 2013). Investigation of the surface energy balance of the Devon Ice Cap between 2007 and 2010 found increases in summer (JJA) melt energy were associated with an increase in net shortwave radiation in June and July, and with an increase in net longwave radiation in August (Gascon et al., 2013). Strong, persistent anticyclonic circulation maximizes the incoming shortwave radiation received at the air-ice interface, and a lower albedo increases the proportion of incoming solar radiation that is absorbed, providing more energy for warming and melt.~~

Our results show that the bulk of the decline in mean summer QEI albedo occurred in July (Sect. 3.2), which is consistent with previous work (e.g. Alt, 1987; Gardner and Sharp, 2007) that found variability in July near-surface air temperatures to be the primary influence on inter-annual variability in annual QEI mass balance. Variability in July air temperatures has, in turn, been associated with the variations in the strength, position, and geometry of the July circumpolar vortex (Gardner and Sharp, 2007). Extreme high-melt years in the QEI are associated with the intrusion of a steep ridge at all levels in the troposphere and the absence of the North American trough, making the QEI thermally homogeneous with continental North America (Alt, 1987). Between 2001 and 2016, in warm years with low (e.g. 2007-2012) (high (e.g. 2001-2004)) albedos, there was a persistent ridge (trough) in the 500 hPa geopotential height surface centered over the north and west of the QEI (Fig. 4; Sect. 3.1.1;). This configuration appears to be tied to the increased warming and albedo declines observed in the central western part of the QEI from 2007 to 2012. For example, strong warming and albedo declines over Axel Heiberg Island and north-central Ellesmere Island coincided with a ridge of high pressure centered over the north and west of the QEI that was often observed in years when the NAO index was negative (Fig. 9).

In contrast to June and July, when the largest BSA declines occurred in the west of the QEI, BSA declines in August were largest at low elevations in the maritime regions of eastern Devon Ice Cap, Manson Icefield, and the southwestern Prince of Wales Icefield (Fig. 5). As mentioned in Section 3.2.1, August weather in the QEI tends to be dominated by cyclonic circulation (Alt, 1987; Gascon et al., 2013). Low pressure systems which track from the southwest to the north and northeast are common in August, and they advect warm moist air into the Arctic from the south. In the eastern QEI, orographic uplift of air masses tracking from the southwest, and subsequent adiabatic heating of these air masses when they descend on the eastern sides of ice masses, would bring warm dry air to the eastern (lee) side of the mountains in the eastern QEI, promoting both warming and albedo decline in these regions in August.

Differences in the dominant atmospheric circulation patterns over the course of the summer season are responsible, at least in part, for where and in which month the largest albedo declines occur. Albedo lowering increases the proportion of incoming solar radiation absorbed at the air-ice interface, and thus the energy available to drive further melt and surface albedo decline. Knowing where and when albedo changes are likely to occur in future is, therefore, important for predicting future rates of mass loss from the QEI ice caps. Recent investigations of atmospheric circulation patterns over the QEI (e.g. Gardner and Sharp, 2007) focused on characterization of July temperature and atmospheric conditions, since July is usually the month when melt rates peak. Our results suggest, however, that changes occurring during the month of August are also important, especially as the length of the melt season continues to increase.

Although large-scale circulation patterns appear to explain much of the broad spatial pattern (and seasonal variability) of BSA change, the physiography of the QEI introduces considerable local variation into the way these changes are expressed. Variations in the magnitudes of both inter-annual variability and longer-term changes in annual precipitation, summer melt duration, and melt intensity have previously been associated with distance from moisture sources (Koerner, 1979; Alt, 1987; Wang et al., 2005). Snow accumulation rates in the QEI tend to decrease from east to west, and Baffin Bay is the largest moisture source for the eastern QEI (Koerner, 1979). Summer snowfall events temporarily raise the surface albedo, while

Commented [m36]: Rev. 2
RC 29: Page 13, lines 407-409 Example of content that may be b placed in the beginning of the manuscript.
AR 29: We appreciate your recommendation to include a backgr section or to include some of this material at the beginning of the manuscript. In revising the manuscript, we found that this particu point fit better towards the end as it helps to place the importance relevance of the August BSA change in the context of existing literature.

locally higher fall and winter snow accumulation can delay the exposure of bare ice and firn in the following summer relative to areas with lower accumulation rates. However, although BSA decreases were generally larger in the north and west, equally large decreases occurred at low elevations on Manson Icefield and southeast Prince of Wales Icefield in the eastern QEI. These large BSA decreases at low elevations in the eastern QEI may arise from a decoupling of high and low elevation temperatures in low melt years. For example, Alt (1978) found that, in some years when there was very little melt near the summit of the Devon Ice Cap, the Sverdrup Glacier (lower elevation) experienced very high melt rates. Further, Wang et al. (2005) attributed comparatively high melt rates observed at low elevations on the Prince of Wales Icefield in 2002 to a decoupling of the temperature regimes experienced at high and low elevations, similar to that described by Alt (1978).

4.2 Relationship between albedo change and temperature

During the period 2001-2016, mean summer QEI-wide LST (16-yr average: -3.25 ± 1.73 °C) increased at a rate of 0.046 ± 0.036 °C yr^{-1} (Table 3). The spatial pattern of LST increase (Fig. S7b) is opposite to the pattern of mean summer BSA change, in that BSA decreases were largest at lower elevations where the mean summer BSA was lowest (Fig. 5a), while LST increases were greatest at higher elevations where the mean summer LST is lower. This observation may be explained by the fact that, at lower elevations, where the mean summer LST regularly reached the melting point, there was less potential for warming than at higher elevations (Mortimer et al., 2016). Investigation of the spatial pattern of the relationship between LST and BSA (derived from linear correlations between the 16 year LST and BSA records for each pixel (Sect. 2.3)), shows that, as expected, LST and BSA were negatively correlated over most of the QEI (~99.7% of pixels; Fig. 9). This negative correlation (average correlation coefficient of all pixels: $r = -0.64$, $p < 0.01$) points to a positive ice-albedo feedback which would promote enhanced rates of glacier mass loss from the QEI. In general, correlations were stronger in the north and west of the QEI than in the south and east, with the exception of the northwest Devon Ice Cap (southeast QEI) where large negative correlation coefficients ($r < -0.8$) were also observed.

The nature of the relationship between LST and BSA varies both within and between regions (Fig. 9). In the eastern QEI [Agassiz Ice Cap, Prince of Wales Icefield, and Devon Ice Cap], correlations tended to be stronger on the western continental side of the north-south running mountain range (where BSA declines were also large) than on the eastern maritime slopes. There were, however, some exceptions to this pattern, most notably a low elevation region near Cadogan Inlet (Fig. 9a, black box), eastern Prince of Wales Icefield, where large negative correlations ($r < -0.8$) were observed and BSA and LST changes were both small. The strong negative correlations in the continental interior are likely attributable to the presence of the north-south trending mountain range in eastern Ellesmere and Devon Islands. In the continental interior of eastern Devon and Ellesmere Islands, warming of air and glacier surface temperatures resulted in albedo decreases, leading to further surface warming. Koerner (1979) attributed the existence of a dry area with low amounts of snow accumulation centered on western Ellesmere Island to the precipitation-shadowing effect of the mountains to the east. In June and July when circulation is primarily anticyclonic, the presence of a barrier to moisture transport from the east limits precipitation on the western (lee)

side of the eastern ice masses, while adiabatic heating of descending air masses results in warm dry air which promotes warming and melting, and enhances albedo decline, in the west.

The strength of the relationship between LST and BSA also varies with elevation. Correlations tended to be weaker and more variable at high elevations, although there are also several instances of low correlations at low elevations, for instance on southeast Devon Ice Cap and Manson Icefield. At lower elevations, where the mean summer LST is high (Fig. S7a), weaker correlations between temperature and albedo may reflect the fact that the albedo continues to decline once the surface temperature has reached the melting point. At high elevations (above ~1500 m a.s.l., Sect. 3.2) BSA decreases were small or non-existent, and the correlation between LST and BSA was both modest and highly variable (Fig. 9). Moderate negative correlations ($r > -0.6$) and some instances of positive correlations, were observed at high elevations on Prince of Wales Icefield and Agassiz Ice Cap. On northwest Ellesmere Island where correlations were generally strongly negative, high-elevation regions had more moderate correlations and some instances of positive correlations between LST and BSA were also observed. LST increases were largest at high elevations (Fig. S7b) and melt occurred at all elevations and at all locations in the QEI at some point during the 2000-2015 period (Mortimer et al., 2016). Since the rate of grain metamorphism increases with the temperature and water content of snow, even warmer summer temperatures may be needed to promote large-scale albedo decline in permanently snow-covered high elevation areas. Alternatively, higher air temperatures in such regions may promote increased summer snowfall and more frequent riming events, which temporarily raise the surface albedo and limit long-term albedo decline. We note that in many high elevation regions, where BSA changes were either small or not observed and correlations between LST and BSA were weak and highly variable, PC1 had positive component scores (compared with negative scores elsewhere). Although PC1 was strongly correlated with the summer NAO index (Sect. 3.3), the occurrence of positive component scores in these high elevation regions (compared with large negative scores elsewhere) may point to an additional mechanism that is affecting the albedo record in these regions. Variability in the extent of open water in the QEI's inter-island channels has previously been correlated with variability in summer temperatures and 500 hPa geopotential height anomalies in the QEI (Koerner, 1977; Bezeau et al., 2015). Increased open water extent during warm years promotes atmospheric convection, which strengthens the advection of warm moist air masses into Baffin Bay (Koerner, 1979). In the eastern QEI, the high elevation regions of eastern Ellesmere and Devon Islands act as a barrier to this increased moisture transport (Koerner, 1979). As a result, precipitation is deposited on the eastern maritime slopes, where it temporarily increases the surface albedo. This scenario provides a plausible explanation for lower rates of BSA decline and poor correspondence between LST and BSA changes at higher elevations in the eastern QEI. A similar set of processes may also be occurring at high elevations on northern Ellesmere Island where the Arctic Ocean is the primary moisture source.

5 Conclusions

This study presents the first complete picture of mean summer surface albedo variations over all glaciated surfaces in the QEI during the period 2001-2016. Mean summer shortwave broadband black-sky albedo decreased at a rate of 0.0029 ± 0.0025 yr

[1] over the 16-year period. Strong negative BSA anomalies from 2007-~~20~~12 suggest that the bulk of the observed albedo decline occurred during this six-year period. Large albedo declines occurred in July (-0.0050 ± 0.0031 yr^{-1}); while no change in BSA occurred in either June or August, indicating that the bulk of the mean summer BSA decrease is concentrated in July~~,~~ when strong anticyclonic circulation occurs. The 16-year history of mean summer BSA changes is strongly tied to variations in the summer NAO index, except in the years 2006, 2010, and 2016 when changes in the mean summer BSA appear to be dominated by the effect of changes in the mean August BSA. Albedo declines were largest at low elevations around the margins of the ice masses and the 16-year record of mean summer BSA was negatively correlated with the 16 year record of mean summer LST ~~(which increased at a rate of 0.046 ± 0.036 °C yr^{-1} during the 2001-2016 period), indicating~~ suggesting the ~~presence~~ existence of a positive ice-albedo feedback ~~in a warming climate~~ that would enhance rates of glacier mass loss from the QEI in a warming climate.

Albedo declines increase the proportion of incoming solar radiation absorbed at the air-ice interface, and thus the energy available to drive melt, warming, and further surface albedo decline. Warmer temperatures, in turn, increase the rate of snow grain metamorphism which lowers the albedo. Air and surface temperatures affect the removal (timing and extent) of the seasonal snowpack which exposes lower albedo firn and/or glacier ice, while melting glacier ice releases impurities that further reduce its albedo. Given that temperature and albedo are inextricably linked, ~~Differences in the dominant atmospheric circulation patterns over the course of the summer season are responsible, at least in part, for where and in which month the largest albedo declines occur. Albedo lowering increases the proportion of incoming solar radiation absorbed at the air-ice interface, and thus the energy available to drive further melt and surface albedo decline. K~~knowing where and when albedo changes are likely to occur in future is, therefore, important for predicting future rates of mass loss from the QEI ice caps. Recent investigations of atmospheric circulation patterns over the QEI (e.g. Gardner and Sharp, 2007) focused on characterization of July temperature and atmospheric conditions, since July is usually the month when melt rates peak. Our results suggest, however, that changes occurring during the month of August are also important, especially as the length of the melt season continues to increase.

Data availability. MODIS data are available from https://lpdaac.usgs.gov/. NCEP/NCAR R1 Reanalysis data are available from http://www.esrl.noaa.gov/psd/data/gridded/.

Competing interests. The authors declare that they have no conflict of interest.

Acknowledgements We thank NSERC Canada (Discovery Grant to MS, Vanier Canada Postgraduate Scholarship to CM), and Alberta Innovates – Technology Futures (MS) for financial support. Scott Williamson provided helpful advice on MODIS data processing and Bert Wouters for providing 2016 GRACE data. ~~MODIS data are available from https://lpdaac.usgs.gov. NCEP/NCAR R1 Reanalysis data are available from http://www.esrl.noaa.gov/psd/data/gridded/).~~

Commented [CM37]: Rev. 1
RC: Though they point out that albedo and LST are negatively correlated for the QEI, they do not discuss that relationship as ca and-effect in either the Abstract or the Conclusion. The relationsl between albedo and LST is discussed in Section 4.2 but I would l liked that discussion to have been better integrated throughout th paper.
AC: Additional text regarding the relationship between temperatu and albedo has been included in the conclusion.

References

Ackerman, S. A., Strabala, K. I., Menzel, P. W., Frey, R. A., Moeller, C. C., and Gumley, L. E.: Discriminating clear sky from clouds with MODIS, J. Geophys. Res., 103(D24), 32141–32157, doi:10.1029/1998JD200032, 1998.

Alexander, P. M., Tedesco, M., Fettweis, X., van de Wal, R. S. W., Smeets, C. J. P. P., and van den Broeke, M. R.: Assessing spatiotemporal variability and trends in modeled and measured Greenland Ice Sheet albedo (2000-2013), The Cryosphere, 8(6), 2293-2312, doi: 10.5194/tc-8-2293-2014, 2014.

Alt, B. T.: Synoptic climate controls of mass-balance variations on Devon Island Ice Cap, Arct. Alp. Res., 10(1), 61–80, doi:10.2307/1550657, 1978.

Alt, B. T.: Developing synoptic analogs for extreme mass balance conditions on Queen Elizabeth Island ice caps, Journal of Applied Climate, 26(12), 1605-1623, doi: 10.1175/1520-0450(1987)026<1605:DSAFEM>2.0.CO;2, 1987.

Arendt, A., et al.: Randolph Glacier Inventory Vers. 3.0: *a dataset of Global Glacier Outlines*. Global Land Ice Measurements from Space, Boulder, CO. Digital media: http//www.glims.org/RGI/rgi32_dl.html, 20132.

Barnes, W. L., Pagano, T.S., and Salomonson V.V.: Prelaunch characteristics of the Moderate Resolution Imaging Spectroradiometer (MODIS) on EOS-AM1, IEEE Transactions on Geoscience and Remote Sensing, 36(4), 1088-1100, doi: 10.1109/36.700993, 1998.

Bezeau, P., Sharp, M. and Gascon, G.: Variability in summer anticyclonic circulation over the Canadian Arctic Archipelago and west Greenland in the late 20th/early 21st centuries and its effects on glacier mass balance, Int. J. Climatol, 35(4), 540-557, doi:10.1002/joc.4000, 2015.

Box, J. E., Fettweis, X., Stroeve, J. C., Tedesco, M., Hall, D. K., and Steffen, K.: Greenland ice sheet albedo feedback: thermodynamics and atmospheric drivers, The Cryosphere, 6(4), 821-839, doi: 10.5194/tc-6-821-2012, 2012.

Box, J. E., van As D., and Steffen, K.: Greenland, Canadian and Icelandic land ice albedo grids (2000-2016), Geological Survey of Denmark and Greenland Bulletin, 38, 69-72, 2017.

Braithwaite, R. J.: Mass balance characteristics of arctic glaciers, Ann. Glaciol., 42, 225-229, doi: 10.3189/17275640578182899, 2005.

Casey, K. A., Polashenski, C. M., Chen, J., and Tedesco, M.: Impact of MODIS sensor calibration updates on Greenland Ice Sheet surface reflectance and albedo trends, The Cryosphere, 11, 1781-1795, doi: 10.5194/tc-11-1781-2017, 2017.

Clarke, A. D., and Noone, K. J.: Soot in the Arctic snowpack: a cause for perturbations in radiative transfer, Atmospheric Environment, 19(12), 2045-2053, doi: 10.1016/0004-6981(85)90113-1, 1985.

Colbeck, S. C.: An overview of seasonal snow metamorphism, Rev. Geophys., 20(1), 45-61, doi: 10.1029/RG020i001p00045, 1982.

Conway, H., Gades, A., and Raymond, C. F.: Albedo of dirty snow during conditions of melt, Water Resour. Res, 32(6), 1716-1718, doi: 10.1029/96WR00712, 1996.

Cuffey, K. M., and Paterson, W. (Eds.): The physics of glaciers, 4th edn. Butterworth-Heinemann, Oxford, 2010.

Doherty, S. J., Warren, S. G., Grenfell, T. C., Clarke, A. D., and Brandt, R. E.: Light absorbing impurities in Arctic snow, Atmos. Chem Phys, 10(23), 11647-11680, doi: 10.5194/acp-10-11647-2010, 2010.

Flanner, M. G., Zender, C. S., Randerson, J. T., and Rasch, P. J.: Present-day climate forcing and response from black carbon in snow, J. Geophys. Res., 112, D11202, doi:10.1029/2006JD008003, 2007.

Fountain, A.G., Tranter, M., Nylen, T. H., and Muller, D. R.: Evolution of cryoconite holes and their contribution to meltwater runoff from glaciers in the McMurdo Dry Valleys, Antarctica, J. Glaciol, 50(168), 35-45, doi: 10.3189/172756504781830312, 2004.

Franz, B.A., Kwiatkowska, E.J., Meister, G. and McClain, C.R.: Moderate Resolution Imaging Spectroradiometer on Terra: limitations for ocean color applications, Journal of Applied Remote Sensing, 2(1), 023525, doi: 10.1117/1.2957964, 2008.

Gardner, A. S., and Sharp, M.: Influence of the Arctic circumpolar vortex on the mass balance of Canadian High Arctic glaciers, J. Clim., 20(18), 4586-4598, doi10.1175JCLI4268.1, 2007.

Gardner, A. S., Moholdt, G., Wouters, B., Wolken, G. J., Burgess, D. O., Sharp, M. J., Braun, C., Labine, C.: Sharply increased mass loss from glaciers and ice caps in the Canadian Arctic Archipelago, Nature, 473(7347), 357-360, doi: 10.1038/nature10089, 2011.

Gardner, A. S., Moholdt, G., Cogley, G., Wouters, B., Arendt, A. A., Wahr, J., Berthier, E., Hock, R., Pfeffer, W. T., Kaser, G., Ligtenberg, S. R. M., Bolch, T., Sharp, M., Hagen, J. O., van den Broeke, M. R., and Paul, F.: et al.: A reconciled estimate of glacier contributions to sea level rise: 2003 to 2009, Science, 340(6134), 852-857, doi:10.1126/science.1234532, 2013.

Gascon, G., Sharp, M., and Bush, A.: Changes in melt season characteristics on Devon Ice Cap, Canada, and their association with the Arctic atmospheric circulation, Ann. Glaciol., 54, 101–110, doi:10.3189/2013AoG63A601, 2013.

Guenther, B., Barnes, W., Knight, E., Barker, J., Harnden, J., Weber, R., Roberto, M., Godden, G., Montgomery, H., and Abel, P.: MODIS calibration: a brief review of the strategy for the at-launch calibration approach, Journal of Atmospheric and Oceanic Technology, 13(2), 274-285. doi: 10.1175/1520-0426(1996)013<0274:MCABRO>2.0.CO;2, 1996.

Guenther, B. Godden, G. D., Xiong, X., Knight, E.J., Qiu, S. Y., Montgomery, H., Hopkins, M. M., Khayat, M. G., and Zhidong Hao, Z.: Prelaunch algorithm and data format for the Level 1 calibration products for the EOS-AM1 Moderate Resolution Imaging Spectroradiometer (MODIS), IEEE Transactions on Geoscience and Remote Sensing, 36(4), 1142-1151, doi: 10.1109/36.701021, 1998.

Hall, D. K., Riggs, G. A., Salomonson V. V. DiGirolamo N. E., Bayr K. J.: MODIS snow-cover products, Remote Sens. Environ., 83(1), 181-194, doi: 10.1016/S0034-4257(02)00095-0, 2002.

Hall, D. K., Box, J. E., Casey, K. A., Hook, S. J., Shuman, C. A., and Steffen, K.: Comparison of satellite-derived and in-situ observations of ice and snow surface temperatures over Greenland, Remote Sens. Environ., 112(10), 3739-3749, doi: 10.1016/j.rse.2008.05.007, 2008~~b~~a.

Hall, D. K., Williams, R. S., Luthcke, S. B., and DiGirolamo, N. E.: Greenland ice sheet surface temperature, melt and mass loss: 2000–2006, J. Glaciol., 54(184), 81–93, doi:10.3189/002214308784409170, ~~2008a~~2008b.

~~Hall, D. K., Box, J. E., Casey, K. A., Hook, S. J., Shuman, C. A., and Steffen, K.: Comparison of satellite-derived and in-situ observations of ice and snow surface temperatures over Greenland, Remote Sens. Environ., 112(10), 3739-3749, doi: 10.1016/j.rse.2008.05.007, 2008b.~~

Hall, D. K., Comiso, J. C., DiGirolamo, N. E., Shuman, C. A., Key, J. R., and Koenig, L. S.: A satellite-derived climate-quality data record of the clear-sky surface temperature of the Greenland ice sheet, J. Clim., 25, 4785-4798, doi: 10.1175/JCLI-D-11-00365.1, 2012.

He, T., Lian, S. L., and Song, D. X.: Analysis of global land surface albedo climatology and spatial-temporal variation during 1981-2010 from multiple satellite products, J. Geophys. Res.-Atmos., 119(17), 10281-10298, doi: 10.1002/2014/JD021667, 2014.

Jin, Y., Schaaf, C. B., Woodcock, C. E., Gao, F., Li, X., and Strahler, A. H.: Consistency of MODIS surface BRDF/Albedo retrievals: 1. Algorithm performance, J. Geophys. Res. 108(D5), 4158, doi: 10.1029/2002JD002803, 2003.

Justice, C.O., Vermote, E., Townshend, J.R.G., Defries, R., Roy, D. P., Hall, D. K., Vincent V. Salomonson V. V. et al.: The Moderate Resolution Imaging Spectroradiometer (MODIS): Land remote sensing for global change research, IEEE Transactions on Geoscience and Remote Sensing, 36(4), 1228-1249, doi: 10.1109/36.701075, 1998.

Kalnay, E., Kanamitsu, M., Kistler, R., Collins, W., Deaven, D., Gandin, L., Iredell, M., Saha, S., White, G., Woollen, J., Zhu, Y., Leetmaa, A., Reynolds, R., Chelliah, M., Ebisuzaki, W., Higgins, W., Janowiak, J., Mo, K.C., Ropelewski, C., Wang, J., Jenne, R., and Joseph, D.: The NCEP/NCAR 40 year reanalysis project, Bull. Am. Meteorol. Soc., 77(3), 437–471, doi:10.1175/1520-0477(1996) 077<0437:TNYRP>2.0.CO;2, 1996.

King, M. D., Platnick, S., Yang, P., Arnold, G. T., Gray, M. A., Ridei, J. C., Ackerman, S. A., and Liu, K. N.: Remote Sensing of Liquid Water and Ice Cloud Optical Thickness and Effective Radius in the Arctic: Application of Airborne Multispectral MAS Data, J. Atmos. Ocean. Technol., 21(6), 857–875, doi:10.1175/1520-0426(2004)021<0857:RSOLWA>2.0.CO;2, 2004.

Koenig, L. S., and Hall, D. K.: Comparison of satellite, thermochron and station temperatures at Summit, Greenland, during the winter of 2008/09, J. Glaciol., 56(198), 735-741, (doi: 10.3189/002214310793146269), 2010.

Koerner, R. M.: Devon Island ice cap: core stratigraphy and paleoclimate, Science, 196(4285), 15-18, doi: 10.1126/science.196.4285.15, 1977.

Koerner, R. M.: Accumulation, ablation, and oxygen isotope variations on the Queen Elizabeth Islands ice caps, Canada, J. Glaciol., 22(86), 25-41, 1979.

Koerner, R. M.: Mass balance of glaciers in the Queen Elizabeth Islands, Nunavut, Canada, Ann. Glaciol., 42, 417–423, doi:10.3189/172756405781813122, 2005.

Kwiatkowska, E. J., Franz, B. A., Meister, G., McClain, C. R., and Xiong, X.: Cross calibration of ocean-color bands from Moderate-Resolution Imaging Spectroradiometer on Terra platform, Applied Optics, 47(36), 6796–6810, doi:10.1364/AO.47.006796, 2008.

Land Processes Distributed Active Archive Center (LP DAAC), MODIS Level 3 Global 1 km Grid SIN Version 56. NASA EOSDIS Land Processes DAAC, USGS Earth Resources Observation and Science (EROS) Center, Sioux Falls, South Dakota (https://lpdaac.usgs.gov), dataset accessed September 2014- October 2015 2017 and June 2017 at http://e4ftl01.cr.usgs.gov.

Lenaerts, J. T. M., van Angelen, J.H., van den Broeke, M. R., Gardner, A. S., Wouters, B., and van Meijgaard, E.: Irreversible mass loss of Canadian Arctic Archipelago glaciers, Geophys. Res. Lett., 40(5), 870–874, doi:10.1002/grl.50214, 2013.

Liu, J., Schaaf, C. B., Strahler, A. H., Jiao, Z., Shuai, Y., Zhang, Q., Román, M., Augustine, J. A., and Dutton, E. G.: Validation of Moderate Resolution Imaging Spectroradiometer (MODIS) albedo retrieval algorithm: Dependence of albedo on solar zenith angle, J. Geophys. Res.-Atmos., 114, D01106, doi:10.1029/2008JD009969, 2009.

Lucht, W., Schaaf, C. B., and Strahler, A. H.: An algorithm for the retrieval of albedo from space using semiempirical BRDF models, IEEE Transactions on Geoscience and Remote Sensing, 38, 977-998, 2000.

Lyapustin, A., Wang, Y., Xiong, X., Meister, G., Platnick, S., Levy, R., Franz, B., Korkin, S., Hilker, T., Tucker, J., Hall, F., Sellers, P., Wu, A., and Angal, A.: Scientific impact of MODIS C5 calibration degradation and C6+ improvements, Atmos. Meas. Tech., 7(12), 4353-4365, doi:10.5194/amt-7-4353-2014, 2014.

Mortimer, C. A., Sharp, M., and Wouters, B.: Glacier surface temperatures in the Canadian high arctic, 2000-2015, J. Glaciol., 62(23), 963-975, doi: 10.1017/jog.2016.80, 2016.

Pan C., Xiong, X., Che, N.: MODIS pre-launch characterization of reflective solar bands response vs. Scan angle, Proc. SPIE – Earth Observeing Systems XII, Optical Engineering Applications, 66770R, doi:10.117/12.730573, 2007.

Pfeffer, W. T., Arendt, A. A., Bliss, A., Bloch, T., Cogley, J. G., Gardner, A. S., Hagen, J. O., Hock, R., Kaser, G., Kienholz, C., Miles, E. S., Moholtd, G., Molg, N., Paul, F., Radic, V., Rastner, P., Raup, B., Rich, J., Sharp, M. J., and The Randolph Consortium: The Randolph Glacier Inventory: a globally complete inventory of glaciers, J. Glaciol., 60(221), 537-552, doi:10.3189/2014JoG13J176, 2014.

Polashenski, C. M., Dibb, J. E., Flanner, M. G., Chen, J. Y., Courville, Z. R., Lai, A. M., Schauer, J. J., Shafer, M. M., and Bergin, M.: Neither dust nor black carbon causing apparent albedo decline in Greenland's dry snow zone: Implications for MODIS C5 surface reflectance, Geophys. Res. Lett., 42(12), 9319-9327, doi: 10.1002/2015GL065912, 2015.

Rajewicz, J., and Marshall, S. J.: Variability and trends in anticyclonic circulation over the Greenland ice sheet, 1948-2013, Geophys. Res. Lett., 41(8), 2842-2850, doi:10.1002/2014GL059255, 2014.

Salomon, J. G., Schaaf, C. B., Strahler, A. H., Gao, F., and Jin, Y.: Validation of the MODIS Bidirectional Reflectance Distribution Function and Albedo retrievals using combined observations from the Aqua and Terra platforms, IEEE Transactions on Geoscience and Remote Sensing, 44(6), 1555-1565, 2006.

Schaaf, C. B., Gao, F., Strahler, A. H., Lucht, W., Li, X., Tsang, T., Strugnell, N. C., Zhang, X., Jin, Y., Muller, J. P., Lewis, P., Barnsley, M., Hobson, P., Disney, M., Roberts, G., Dunderdale, M., Doll, C., d'Entremont, R. P., Hu, B., Liang, S., Privette, J. L., and Roy, D.: First operational BRDF, albedo nadir reflectance products from MODIS, Remote Sens. Environ., 83(1), 135-148, doi: 10.1016/S0034-4257(02)00091-3, 2002.

Schaaf, C. B., Wang, Z., and Strahler, A. H.: Commentary on Wang and Zender – MODIS snow albedo bias at high solar zenith angles relative to theory and in situ observations in Greenland, Remote Sens. Environ., 115(5), 1296-1300, doi: 10.1016/j.rse.2011.01.002, 2011.

Schaaf, C., and Wang, Z.: MCD43A3 MODIS/Terra+Aqua BRDF/Albedo Daily L3 Global - 500m V006. NASA EOSDIS Land Processes DAAC. dataset accessed November 2016 at doi:10.5067/MODIS/MCD43A3.006, 2015.

Sharp, M., Burgess, D. O., Cogley, J. G., Ecclestone, M., Labine, C., and Wolken, G. J.: Extreme melt on Canada's Arctic ice caps in the 21st century, Geophys. Res. Lett., 38(11), L11501, doi:10.1029/2011GL047381, 2011.

Strabala, K. I., Ackerman, S. A., and Menzel, W. P.: Cloud Properties inferred from 8–12 μm Data, J. Appl. Meteor., 33(2), 212–229, doi:10.1175/15200450(1994)033<0212:CPIFD>2.0.C;2, 1994.

Commented [m38]: Rev. 1
RC 14 Line 601: should read IEEE instead of IEE
AR 14 Reference corrected

Stroeve, J. C., Box, J., Gao, F., Liang, S., Nolin, A., and Schaaf, C.: Accuracy assessment of the MODIS 16-day albedo product for snow: Comparison with Greenland in situ measurements, Remote Sens. Environ., 94(1), 46-60, doi: 10.1016/j.rse.2004.09.001, 2005.

Stroeve, J. C., Box, J., and Haran, T.: Evaluation of the MODIS (MOD10A1) daily snow albedo product over the Greenland Ice Sheet, Remote Sens. Environ., 105(2), 155-171, doi: 10.1016/j.rse.2006.06.009, 2006.

Stroeve, J., Box, J. E., Wang, Z., Schaaf, C., and Barret, A.: Re-evaluation of MODIS MCD43 Greenland albedo accuracy and trends, Remote Sens. Environ., 138, 199-214, doi: 10.1016/j.rse.2013.07.023, 2013.

Strugnell, N., and Lucht, W.: Continental-scale albedo inferred from AVHRR data, land cover class and field observations of typical BRDFs, J. Clim, 14(7), 1360-1376, doi: 10.1175/1520-0442(2001)014<1360:AATICS>2.0.CO;2, 2001.

Sun, J., Xiong, X., Guenther, B., and Barnes, W.: Radiometric stability monitoring of the MODIS reflective solar bands using the Moon, Metrologia, 40(1), S85, doi: 10.1088/0026-1394/40/1/319, 2003.

Sun, J., Xiong, X., Angal, A., Chen, H., Wu, A., and Geng, X.: Time-dependent response versus scan angle for MODIS reflective solar bands, IEEE Transactions on Geoscience and Remote Sensing, 52(6), 3159-3174, doi: 10.1109/TGRS.2013.2271448, 2014.

Tedesco, M., Doherty, S., Fettweis, X., Alexander, P., Jeyaratnam, J., and Stroeve, J.: The darkening of the Greenland ice sheet: trends, drivers, and projections (1981-2100), The Cryosphere, 10, 477-496, doi: 10.5194/tc-10-477-2016, 2016.

Toller, G., Xiong, X., Sun, J., Wenny, B. N., Geng, X., Kuyper, J., Angal, A., Chen, H., Madhavan, S., and Wu, A.: Terra and Aqua moderate-resolution imaging spectroradiometer collection 6 level 1B algorithm, J. Appl. Remote Sens., 7(1), 073557-073557, doi: 10.1117/1.JRS.7.073557, 2013.

van den Broeke, M. R., Smeets, C. J. P. P., and Rvan de Wal, R. S. W.: The seasonal cycle and interannual variability of surface energy balance and melt in the ablation zone of the west Greenland ice sheet, The Crysophere, 5(2), 377-390, doi: 10.5194/tc-5-377-2011, 2011.

Vermote, E. F., Kotchenova, S. Y., and Ray, J. P.: MODIS surface reflectance user's guide. MODIS Land Surface Reflectance Science Computing Facility, version 1, 2011.

Vincent, L. A., Zhang, X., Brown, R. D., Feng, Y., Mekis, E., Milewska, E. J., Wan, H., and Wang, X. L.: Observed trends in Canada's climate and influence of low-frequency variability modes, Journal of Climate, 28, 4545-4560, doi: 10.1175/JCLI-D-14-00697.1, 2015.

Wan, Z., Zhang, Y., Zhang, Q., and Li, Z. L.: Validation of the land-surface temperature products retrieved from Terra Moderate Resolution Spectroradiomerter data, Remote Sens. Environ., 83(1-2), 163-180, doi: 10.1016/S0034-4257(02)00093-7, 2002.

~~Wang L., Sharp, M., Rivard, B., Marshall, S., and Burgess, D.: Melt season duration on Canadian Arctic ice caps, 2000-2004, Geophys. Res. Lett., 32(19), L19502, doi: 10.1029/2005GL023962, 2005.~~

Wang, Z., Schaaf, C. B., Chopping, M. J., Strahler, A. H., Wang, J., Román, M. O., Rocha, A. V., Woodcock, C. E., and Shuai, Y.: Evaluation of Moderate-resolution Imaging Spectroradiometer (MODIS) snow albedo product (MCD43A) over tundra, Remote Sens. Environ., 117, 264-280, doi: 10.1016/j.rse.2011.10.002, 2012.

Wanner, W., Strahler, A. H., Hu, B., Lewis, P., Muller, J. P., Li, X., Schaaf, C. L. B., and Barnsley, M. J..: Global retrieval of bidirectional reflectance and albedo over than from EOS MODIS and MISR data: theory and algorithm, J. Geophys. Res. 102(D14), 17143-17162, doi: 10.1029/96JD03295, 1997.

Warren, S. G.: Optical properties of snow, Reviews of Geophysics, 20(1), 67-89, doi:10.1029/RG020i001p00067, 1982.

Warren, S. G., and Wiscombe, W. J.: A model for the spectral albedo of snow. II Snow containing atmospheric aerosols, J. Atmos. Sci., 37(12), 2734-2745, doi: 10.1175/15200469(1980)037<2734: AMFTSA>2.0.CO;2, 1980.

Wenny, B. N., Sun, J., Xiong, X., Wu, A., Chen, H., Angal, A., Choi, T., Madhavan, S., Geng, X., Kuyper, J., and Tan, L.: MODIS calibration algorithm improvements developed for Collection 6 Level-1B, Proc. SPIE – Earth Observing Systems XV, 78071F, doi: 10.1117/12.860892, 2010.

Wiscombe, W. J., and Warren, S. G.: A model for the spectral albedo of snow. I: Pure snow, J. Atmos. Sci., 37(12), 2712-2732, doi: 10.1175.1520-0469(1980)037<2712:AMFTSA>2.0.CO;2, 1980.

Wolken, G., Sharp, M., Andreassen, L.M., Arendt, A., Burgess, D., Cogley, J.G., Copland, L., Kohler, J., O'Neel, S., Pelto, M., Thomson, L., and Wouters, B.: [Arctic] Glaciers and ice caps outside Greenland [in "State of the Climate 2015"], Bull. Am. Meteorol. Soc., 97(8), S142-S145, 2016.

Xiong, X., Esposito, J., Sun, J., Pan, C., Guenther, B., and Barnes, W. L.: Degradation of MODIS optics and its reflective solar bands calibration, In Proc. SPIE – Sensors, Systems, and Next-Generation Satellites V, 4540, 62-70. Doi: 10.1117/12.450646, 2001.

Xiong, X., Eriyes, H., Xiong, S., Xie, X., Esposito, J., Sun, J., and Barnes, W.: Performance of Terra MODIS solar diffuser and solar diffuser stability monitor, In Proc. SPIE - Earth Observing Systems X, 58820S doi: 10.1117/12.615334, 2005.

960 Xiong, X., and Barnes, W.: An overview of MODIS radiometric calibration and characterization, Advances in Atmospheric Sciences, 23(1), 69-79, doi: 10.1007/s00376-006-0008-3, 2006.

Table 1: Clear-sky BSA and LST; 1 standard deviation. Anomalies are with respect to the 2001-~~20~~16 mean.

Year	BSA mean	BSA mean anomaly*	LST mean	LST mean anomaly*
2001	0.631 ± 0.106	0.0226 ± 0.0458	-3.7 ± 2.0~~-3.9 ± 1.9~~	-0.73 ± 0.70~~-0.65 ± 0.63~~
2002	0.633 ± 0.124	0.0316 ± 0.0320	-3.5 ± 2.2~~-3.7 ± 2.1~~	-0.51 ± 0.68~~-0.43 ± 0.66~~
2003	0.627 ± 0.109	0.0292 ± 0.0329	-3.3 ± 1.9~~-3.9 ± 1.8~~	-0.65 ± 0.51~~-0.65 ± 0.49~~
2004	0.655 ± 0.112	0.0517 ± 0.0318	-4.0 ± 2.4~~-4.2 ± 2.3~~	-1.07 ± 0.80~~-1.00 ± 0.73~~
2005	0.605 ± 0.132	0.0035 ± 0.0282	-2.3 ± 1.7~~-2.6 ± 1.7~~	0.69 ± 0.38~~0.67 ± 0.40~~
2006	0.608 ± 0.120	0.0030 ± 0.0282	-3.9 ± 2.5~~-4.2 ± 2.3~~	-0.94 ± 0.88~~-0.95 ± 0.80~~
2007	0.586 ± 0.125	-0.0167 ± 0.0282	-1.9 ± 1.6~~-2.2 ± 1.6~~	1.06 ± 0.48~~1.00 ± 0.44~~
2008	0.588 ± 0.119	-0.0117 ± 0.0212	-2.4 ± 1.4~~-2.7 ± 1.4~~	0.57 ± 0.53~~0.54 ± 0.52~~
2009	0.586 ± 0.115	-0.0177 ± 0.0220	-2.4 ± 1.7~~-2.8 ± 1.7~~	0.53 ± 0.41~~0.46 ± 0.44~~
2010	0.601 ± 0.112	-0.0021 ± 0.0307	-2.1 ± 1.7~~-2.5 ± 1.7~~	0.86 ± 0.51~~0.77 ± 0.49~~
2011	0.539 ± 0.127	-0.0651 ± 0.0326	-2.0 ± 1.3~~-2.3 ± 1.3~~	0.93 ± 0.67~~0.90 ± 0.61~~
2012	0.550 ± 0.126	-0.0516 ± 0.0309	-2.1 ± 1.4~~-2.4 ± 1.4~~	0.92 ± 0.65~~0.87 ± 0.64~~
2013	0.668 ± 0.086	0.0604 ± 0.0431	-5.2 ± 2.3~~-5.4 ± 2.2~~	-2.26 ± 0.87~~-2.14 ± 0.85~~
2014	0.614 ± 0.109	0.0153 ± 0.0245	-3.2 ± 1.9~~-3.4 ± 1.8~~	-0.18 ± 0.50~~-0.18 ± 0.50~~
2015	0.578 ± 0.124	-0.0223 ± 0.0248	-2.6 ± 1.7~~-2.8 ± 1.7~~	0.37 ± 0.42~~0.37 ± 0.46~~
2016	0.600 ± 0.120	-0.0048 ± 0.0334	-2.5 ± 1.9~~-2.8 ± 1.8~~	0.43 ± 0.66~~0.42 ± 0.68~~
2001-16*	0.599 ± 0.115	–	-3.0 ± 1.8~~-3.2 ± 1.7~~	–

*pixels having mean summer (JJA) BSA observations in at least 11 of a possible 16 years (see Sect. 2.3)

Commented [m39]: Values revised using the C6 instead o C5 LST data.

965

Table 2: Clear-sky mean summer monthly BSA^ and BSA^ anomaly relative to the 2001-16 mean for the QEI ice cover; ± 1 standard deviation.

Year	June	July	August	June anomaly*	July anomaly*	August anomaly*
2001	0.722 ± 0.084	0.584 ± 0.127	0.597 ± 0.123	0.0359 ± 0.0502	0.0285 ± 0.0585	0.0153 ± 0.0572
2002	0.680 ± 0.108	0.615 ± 0.135	0.608 ± 0.145	-0.0005 ± 0.0424	0.0595 ± 0.0435	0.0270 ± 0.0466
2003	0.684 ± 0.085	0.561 ± 0.139	0.658 ± 0.127	0.0003 ± 0.0231	0.0029 ± 0.0340	0.0836 ± 0.0768
2004	0.714 ± 0.085	0.620 ± 0.126	0.632 ± 0.133	0.0317 ± 0.0285	0.0638 ± 0.0465	0.0501 ± 0.0472
2005	0.676 ± 0.099	0.572 ± 0.139	0.573 ± 0.143	-0.0064 ± 0.0300	0.0150 ± 0.0364	-0.0116 ± 0.0468
2006	0.712 ± 0.087	0.615 ± 0.129	0.568 ± 0.137	0.0255 ± 0.0316	0.0602 ± 0.0440	-0.0166 ± 0.0431
2007	0.692 ± 0.090	0.544 ± 0.141	0.536 ± 0.155	0.0099 ± 0.0228	-0.0143 ± 0.0339	-0.0518 ± 0.0494
2008	0.660 ± 0.104	0.533 ± 0.148	0.576 ± 0.118	-0.0220 ± 0.0298	-0.0226 ± 0.0353	-0.0050 ± 0.0345
2009	0.690 ± 0.089	0.536 ± 0.132	0.533 ± 0.142	0.0085 ± 0.0258	-0.0212 ± 0.0310	-0.0544 ± 0.0383
2010	0.668 ± 0.091	0.528 ± 0.136	0.606 ± 0.136	-0.0143 ± 0.0230	-0.0289 ± 0.0331	0.0188 ± 0.0656
2011	0.628 ± 0.101	0.480 ± 0.147	0.521 ± 0.148	-0.0557 ± 0.0347	-0.0770 ± 0.0400	-0.0657 ± 0.0517
2012	0.628 ± 0.112	0.478 ± 0.146	0.559 ± 0.137	-0.0532 ± 0.0395	-0.0805 ± 0.0399	-0.0243 ± 0.0532
2013	0.724 ± 0.072	0.640 ± 0.107	0.628 ± 0.109	0.0402 ± 0.0406	0.0843 ± 0.0517	0.0466 ± 0.0637
2014	0.698 ± 0.080	0.572 ± 0.128	0.584 ± 0.136	0.0167 ± 0.0277	0.0148 ± 0.0335	0.0026 ± 0.0495
2015	0.677 ± 0.103	0.490 ± 0.143	0.587 ± 0.147	-0.0033 ± 0.0282	-0.0675 ± 0.0400	0.0026 ± 0.0457
2016	0.675 ± 0.089	0.545 ± 0.146	0.589 ± 0.146	-0.0066 ± 0.0280	-0.0146 ± 0.0354	0.0049 ± 0.0652
2001-2016*	0.680 ± 0.089	0.551 ± 0.131	0.579 ± 0.127	–	–	–

970 ^average of all pixels in each region having at least 11 (10 for June) of a possible 31 (30 for June) observations.
*pixels having June BSA observations in at least 11 of a possible 16 years.

Table 3: 2001-2016 BSA and LST change for glaciated regions of the QEI (Fig. 1); ± 1 standard deviation.

Year	QEI	Agassiz IC	Axel Heiberg I	Devon I & Coburg I	Manson IF	Meighen IC	Northwest Ellesmere I	Prince of Wales IF	Sydkap IC
JJA Mean BSA ($yr.^{-1}$)	-0.0029 ± 0.0025	-0.0021 ± 0.0022	-0.0041 ± 0.0031	-0.0034 ± 0.0021	-0.0043 ± 0.0026	-0.0055 ± 0.0025	-0.0024 ± 0.0025	-0.0028 ± 0.0021	-0.0036 ± 0.0030
June Mean BSA ($yr.^{-1}$)	-0.0017 ± 0.0024	-0.002 ± 0.0023	-0.0027 ± 0.0027	-0.0019 ± 0.0016	-0.0017 ± 0.0028	-0.0046 ± 0.0017	-0.0011 ± 0.0026	-0.0020 ± 0.0024	-0.0028 ± 0.0022
July Mean BSA ($yr.^{-1}$)	-0.0050 ± 0.0031	-0.0044 ± 0.0026	-0.0077 ± 0.0035	-0.0040 ± 0.0024	-0.0054 ± 0.0028	-0.0081 ± 0.0027	-0.0048 ± 0.0032	-0.0049 ± 0.0028	-0.0064 ± 0.0031
August Mean BSA ($yr.^{-1}$)	-0.0022 ± 0.0036	-0.0010 ± 0.0027	-0.0024 ± 0.0039	-0.0043 ± 0.0036	-0.0057 ± 0.0043	-0.0050 ± 0.0041	-0.0014 ± 0.0032	-0.0016 ± 0.0030	-0.0018 ± 0.0049
JJA LST ($°C\ yr^{-1}$)	0.05 ± 0.04	0.05 ± 0.03	0.07 ± 0.04	0.04 ± 0.03	0.02 ± 0.02	0.07 ± 0.06	0.06 ± 0.03	0.04 ± 0.03	0.04 ± 0.03

Table 3: QEI-wide (regionally-averaged) BSA and LST change for the period 2001-16; ± 1 standard deviation.

JJA Mean BSA ($yr._{-1}$)	June Mean BSA (yr^{-1})	July Mean BSA (yr^{-1})	August Mean BSA (yr^{-1})	JJA LST ($°C\ yr^{-1}$)
-0.0029 ± 0.0025	-0.0017 ± 0.0024	-0.0050 ± 0.0031	-0.0022 ± 0.0036	+0.049 ± 0.038

Commented [m40]: Table revised because regions no long referenced in text.

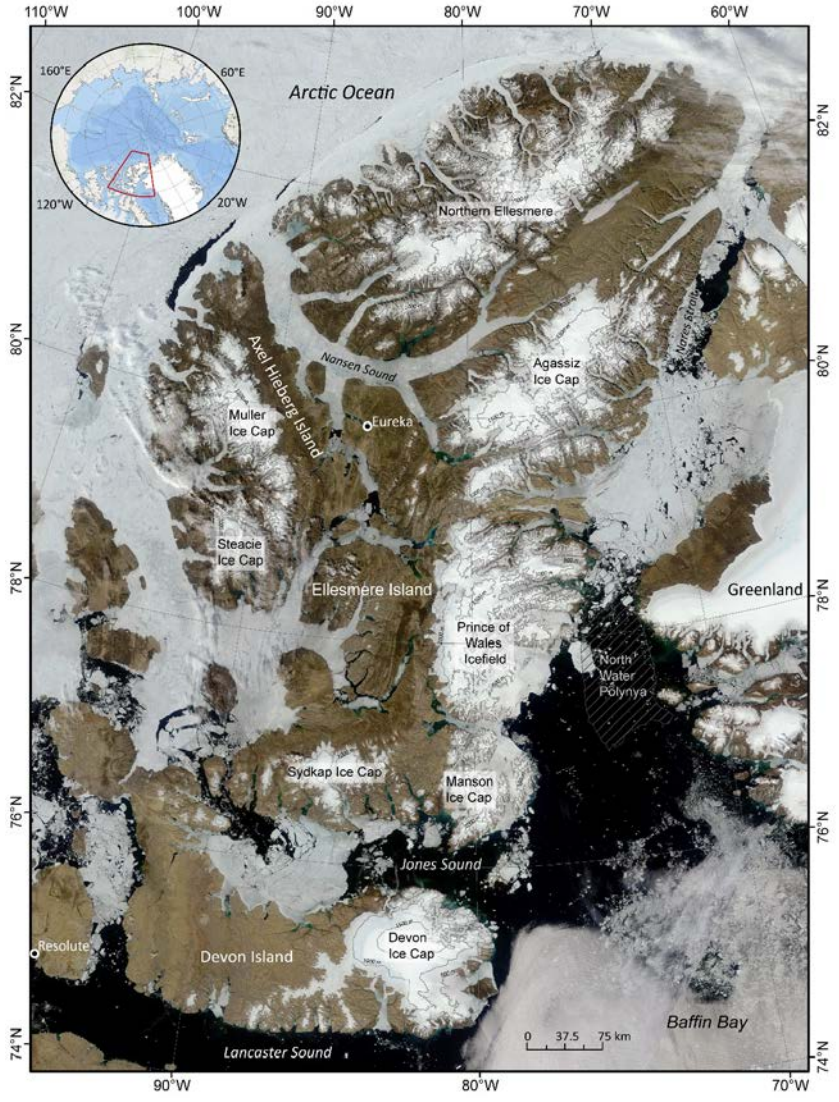
110°W
100°W
90°W
80°W
70°W
60°W
82°N
80°N
78°N
76°N
74°N
160°E
60°E
120°W
20°W
Arctic Ocean
Northern Ellesmere
Nares Strait
Axel Heiberg Island
Nansen Sound
Agassiz Ice Cap
Muller Ice Cap
Eureka
Steacie Ice Cap
Ellesmere Island
Greenland
Prince of Wales Icefield
North Water Polynya
Sydkap Ice Cap
Manson Ice Cap
Jones Sound
Resolute
Devon Island
Devon Ice Cap
Baffin Bay
Lancaster Sound
0 37.5 75 km

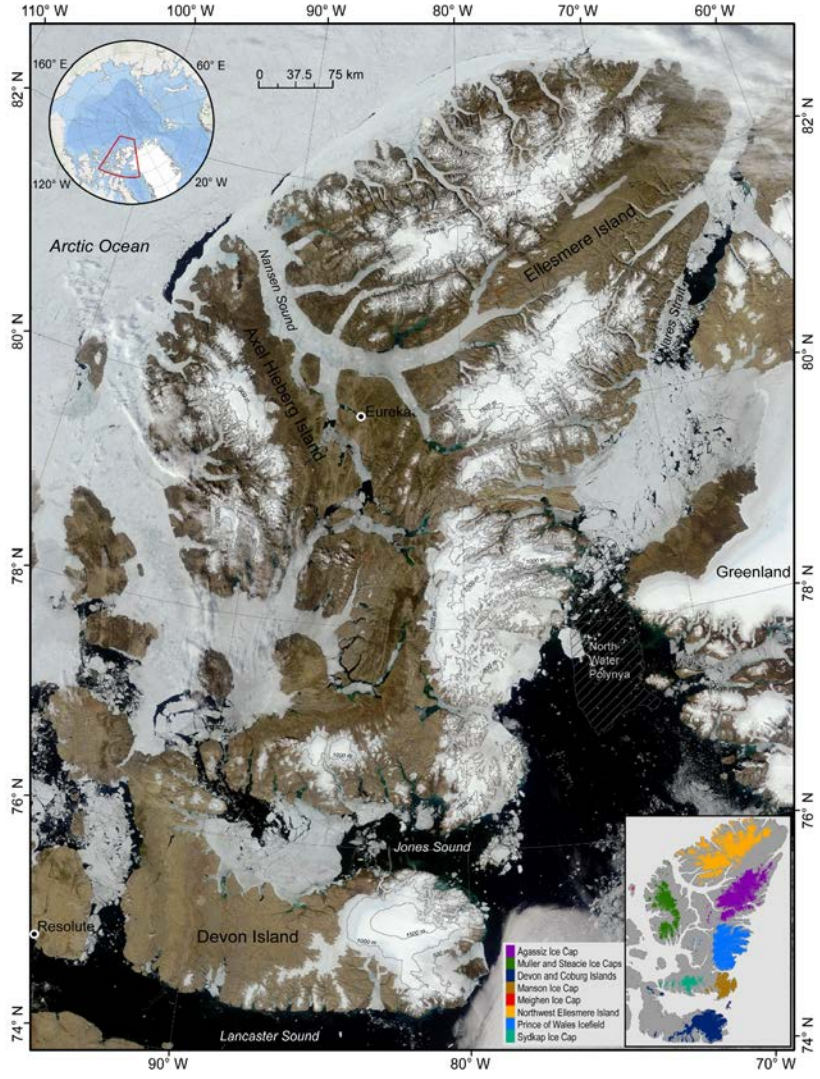

995 **Figure 1: Glaciated regions of the Queen Elizabeth Islands~~, . Arctic Canada.~~ Base Image: Moderate Resolution Imaging Spectroradiometer, 4 July 2011. ~~Top-right I~~inset: red polygon shows location of Queen Elizabeth Islands, Arctic Canada. ~~Bottom-left inset: the eight regions used in this study.~~**

Commented [m41]: Rev. 2
RC 32: Figure 1 image – In some formats, it is difficult to differentiate the thematic colors used in the figure. Consider if th may be other colors to use. For reader friendliness, it may also he move the legend and increase the font size of the legend text. Als consider adding a label to the 8 regions. This may help readers in interpretation of Supplemental Table S2
AR 32: Figure 1 revised. Bottom-right inset no longer included because regional BSA values are no longer referred to in text. La for the major ice masses have been included on the main map. Supplemental Table 2 has been removed.

Commented [m42]: Rev. 2
RC 31: Figure 1 caption – Do the authors intend to reference Moderate Resolution Imaging Spectroradiometer instead of "Moderate Resolution Spectroradiometer"?
AR 31: Figure 1 caption corrected to read Moderate

Commented [m43]: Rev. 1
RC 2: Figure 1 caption: do you mean "Top-left inset" and "Botto right inset"?
AR 2: Bottom-left inset in Figure 1 removed and caption correct

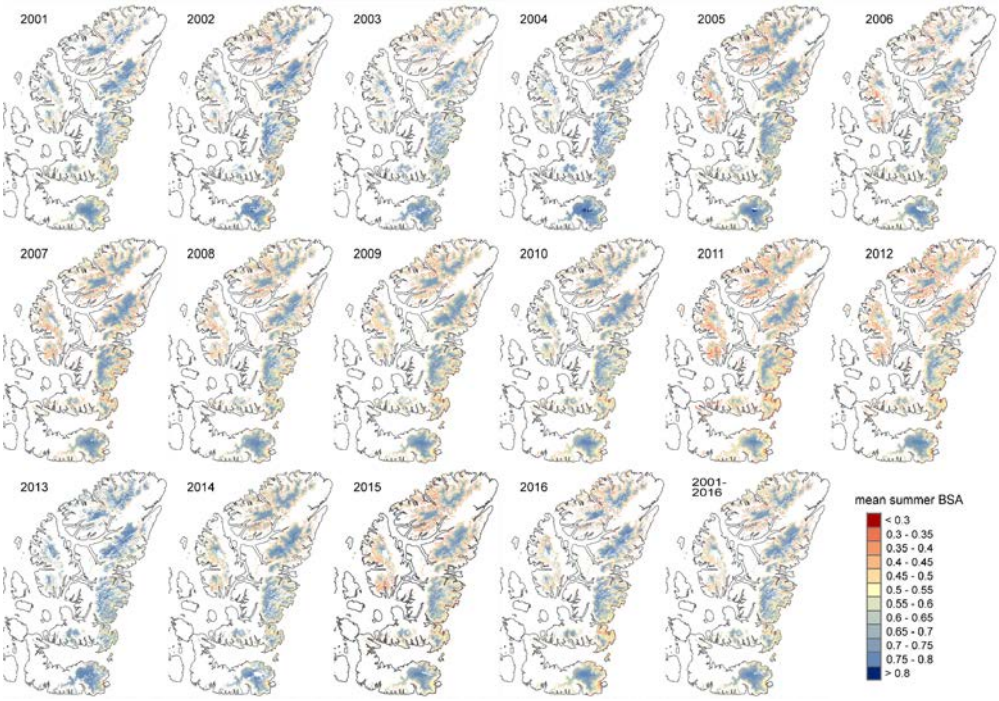

Figure 2: Mean summer clear-sky shortwave broadband black-sky albedo ~~for~~ over the QEI ice caps. White areas outside of the ice caps indicate non-glaciated ice cover.

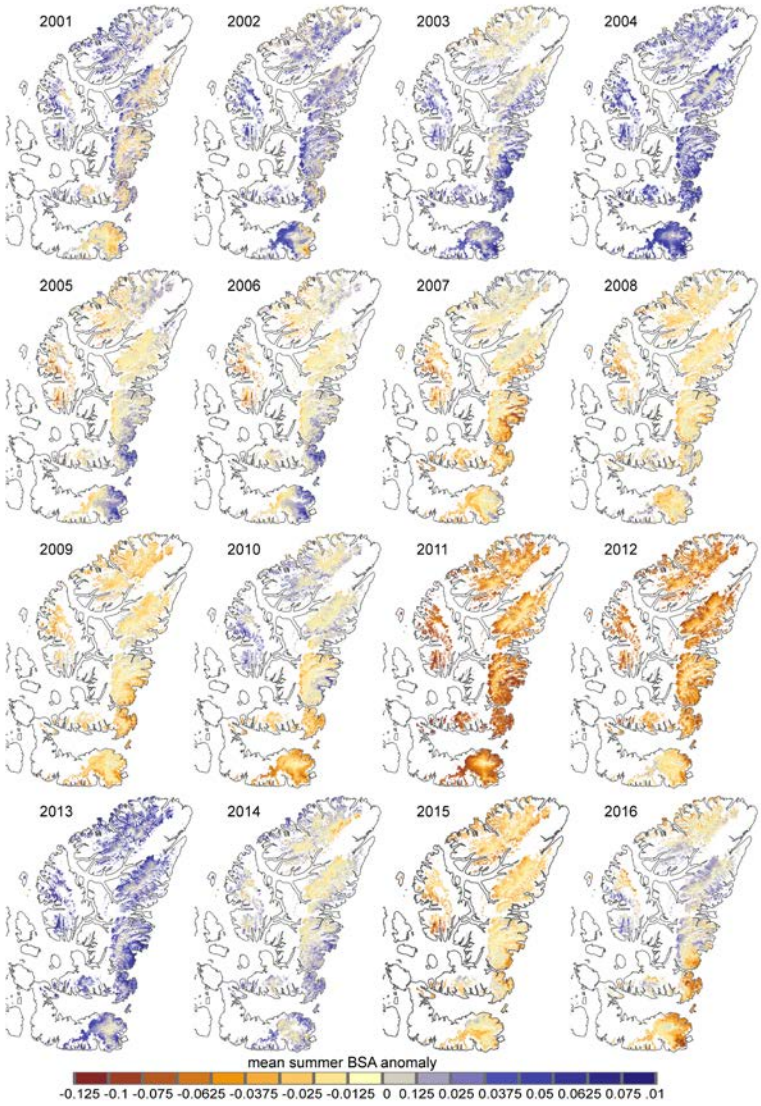

Figure 3: Mean summer clear-sky shortwave broadband albedo anomaly ~~for~~ over the QEI ice caps relative to the 2001-~~20~~16 mean. White areas outside of the ice caps indicate non-glaciated ice cover.

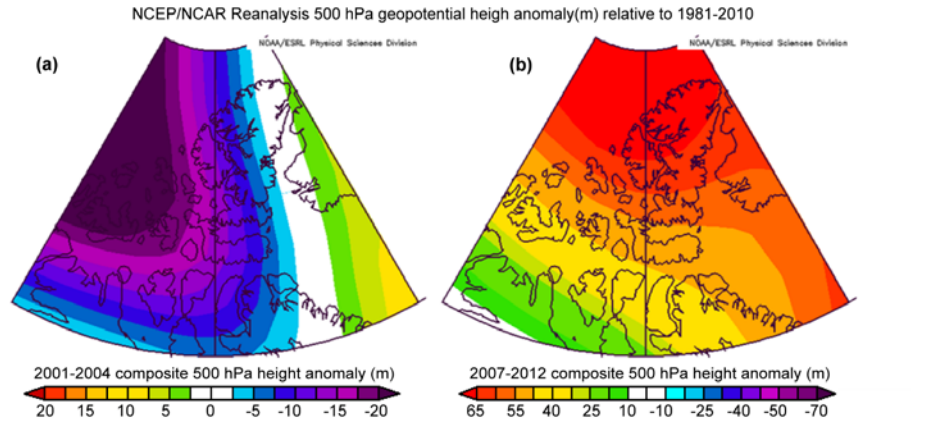

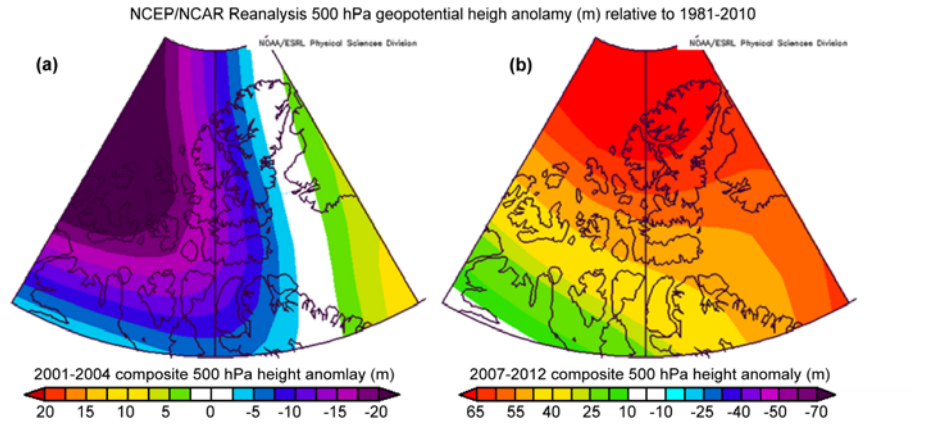

Figure 4: Mean summer (JJA) composite NCEP/NCAR Reanalysis 500 hPa geopotential height anomaly for (a) a period of large negative BSA anomalies (2001-~~20~~04) and (b) a period of large positive BSA anomalies (2007-~~20~~12). Source: https://www.esrl.noaa.gov/psd.

Commented [m44]: Rev. 2
RC 33: Figure 4 – Figure text, misspelled word 'anomaly' in two locations, please correct.
AR 33: Figure 4 correct for two erroneous spellings of 'anomaly'

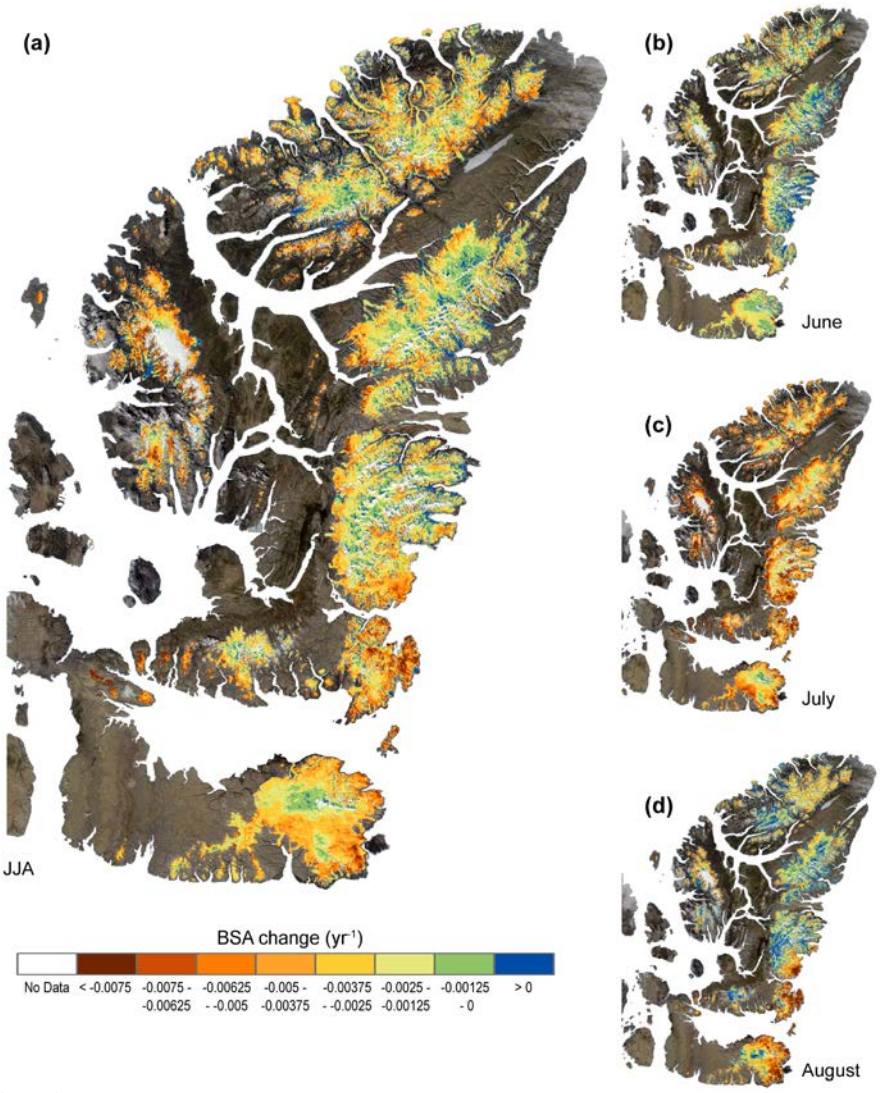

Figure 5: Linear rate of change (yr^{-1}) in (a) mean summer (JJA), (b) June, (c) July, and (b) August, clear-sky shortwave broadband black-sky albedo for 2001-~~20~~16 ~~for~~ over the QEI ice caps. Background image: MODIS 4 July 2011~~.~~. ~~b~~Brown indicates non-glaciated land cover.

Commented [m45]: Rev. 1
RC 3: Figures 2,3,5,6,7&9: it should be mentioned in the caption white (Figs 2 & 3) is not ice and brown is not ice (Figs 5,6,7,&9)
AR 3: Mention of brown (Fig. 5, 6, 7, 9) areas that are not ice ha been added to the figure captions.

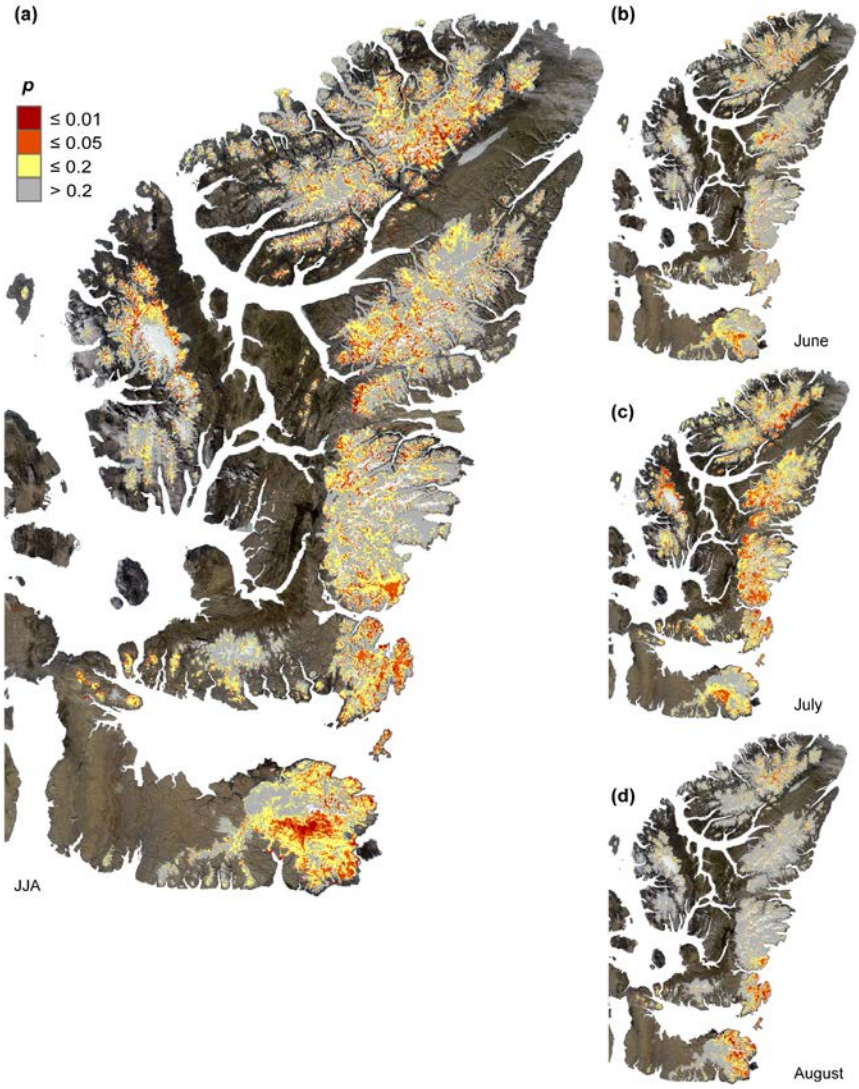

Figure 6: p-value of the linear regression (Fig.4) of (a) mean summer (JJA), (b) June, (c) July, and (~~b~~d) August, clear-sky shortwave broadband black-sky albedo for the period 2001-~~20~~16 ~~for~~ over the QEI ice caps. Background image: MODIS 4 July 2011., ~~b~~Brown indicates non-glaciated land cover.

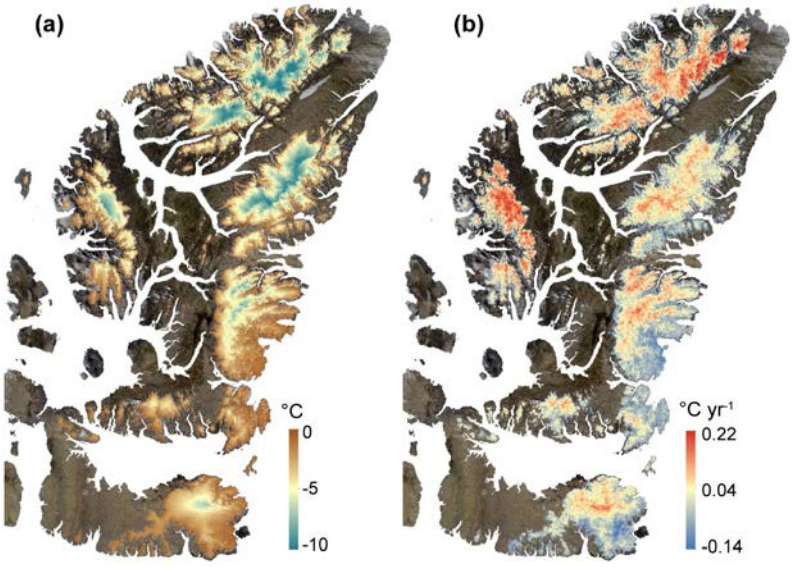

1025

Figure 7: QEI (a) 16 year average mean summer land surface temperature (°C) and (b) linear rate of change of mean summer LST (°C yr^{-1}) for the period 2001-16 over the QEI ice caps. Background image: MODIS 4 July 2011. ~~b~~Brown indicates non-glaciated land cover.

Commented [m46]: Rev. 2
RC 35: Figure S7 – Example of important, interesting QEI LST content for the authors to consider moving from the supplementa material to the main manuscript.
AR 35: Figure S7 moved from supplemental material to the mair and is now Figure 7.

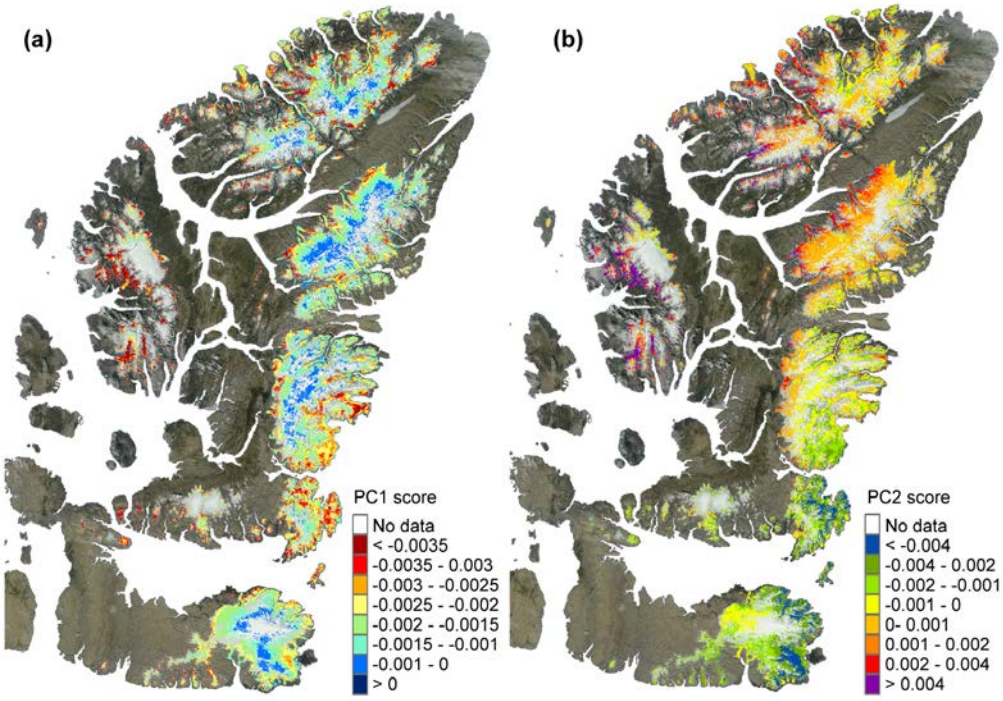
(a)
PC1 score
No data
< -0.0035
-0.0035 - 0.003
-0.003 - -0.0025
-0.0025 - -0.002
-0.002 - -0.0015
-0.0015 - -0.001
-0.001 - 0
> 0
(b)
PC2 score
No data
< -0.004
-0.004 - 0.002
-0.002 - -0.001
-0.001 - 0
0- 0.001
0.001 - 0.002
0.002 - 0.004
> 0.004

1030

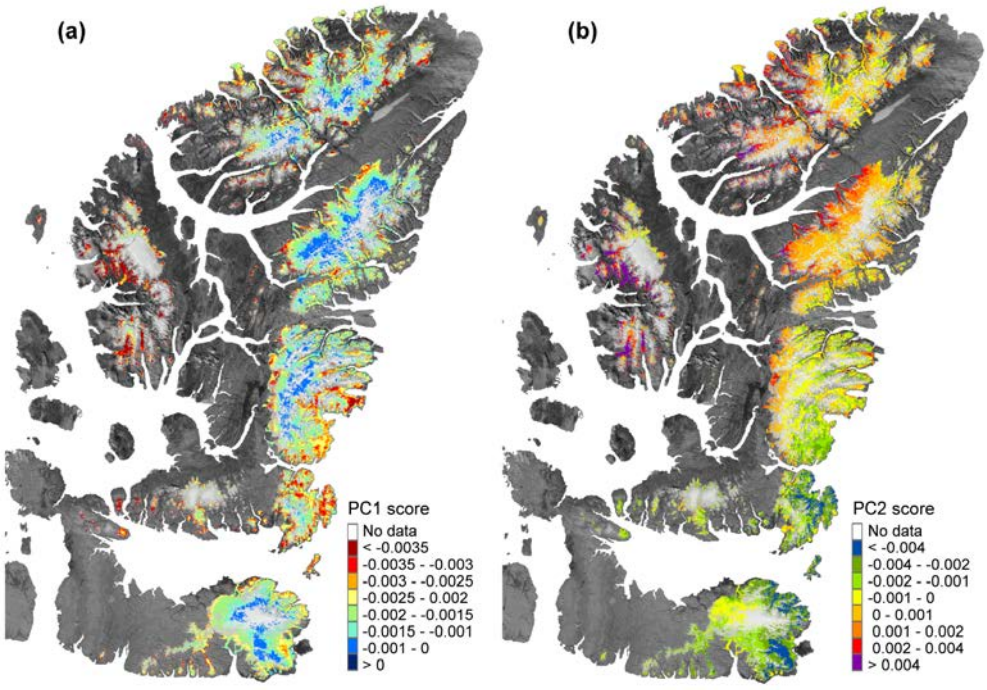

Figure 78: Component scores for the first two Principal Components of the mean summer clear-sky BSA (Fig. 2) ~~for~~ over the QEI ice caps. Background image: MODIS 4 July 2011.~~,~~ B~~b~~rown indicates non-glaciated land cover.

1035

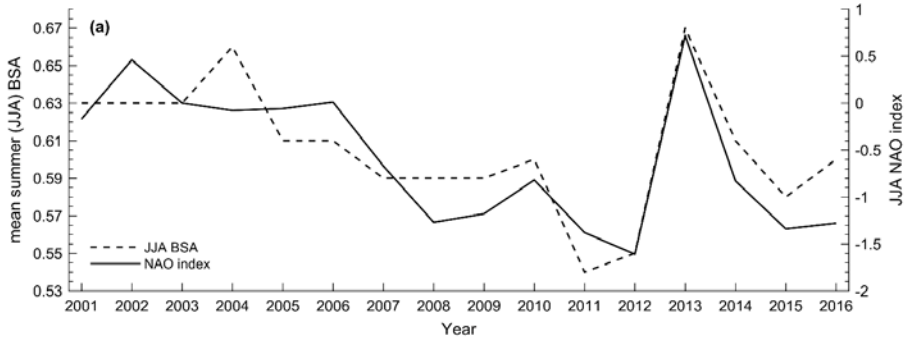
(a)
mean summer (JJA) BSA
JJA NAO index
JJA BSA
NAO index
Year

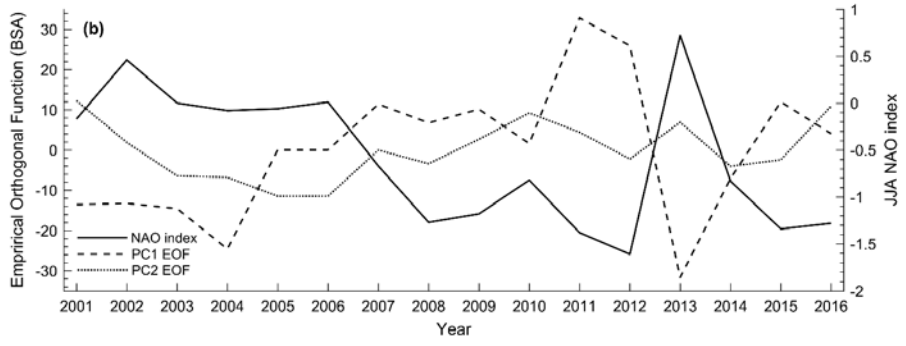
(b)
Emprirical Orthogonal Function (BSA)
JJA NAO index
NAO index
PC1 EOF
PC2 EOF
Year

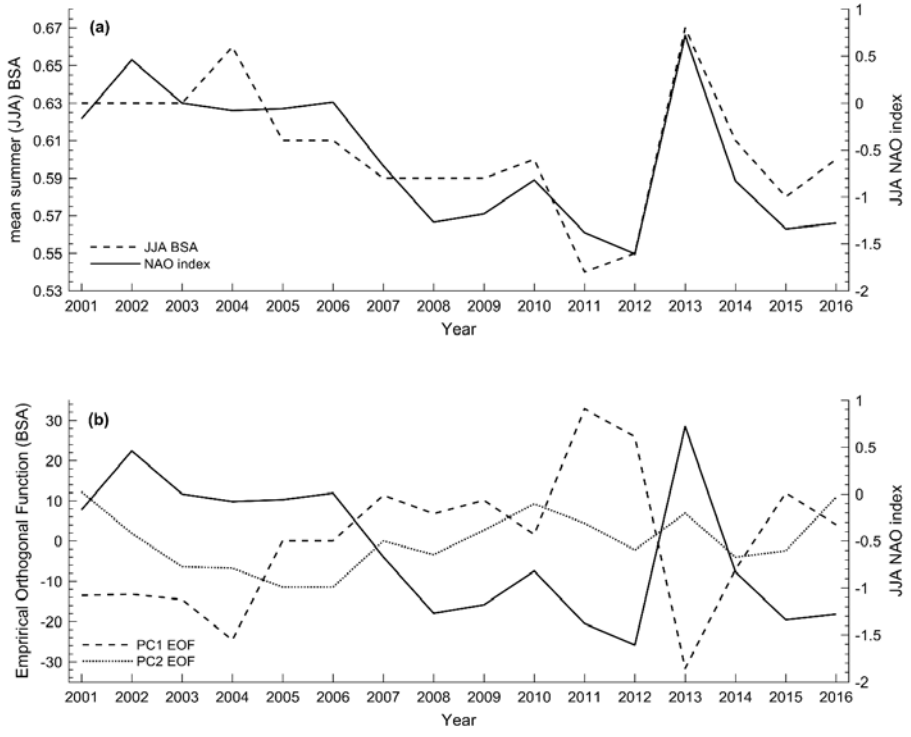

Figure 89: (a) mean summer (JJA) clear-sky shortwave broadband black-sky albedo (left-hand axis) and the mean summer (JJA) NAO index (right-hand axis) for 2001-2016. (b) Empirical Orthogonal Functions (EOF) for the First and Second Principal Components of the 16 year mean summer BSA record (left-hand axis), and the mean summer (JJA) NAO index (right-hand axis) for 2011-2016 (Sect. 3.4).

Commented [m47]: Rev 1.
RC 4: Figure 8 – lower panel: I am confused about the point that are trying to get across in this graph; please clarify.
AR 4: The lower panel of Figure 8 (which is now Figure 9) illust the correspondence between the Empirical Orthogonal Functions the first and second Principal Components of the 16 year mean summer BSA record, respectively, and the mean summer NAO in The graph presents the EOF of PC1 and PC2 of the mean summe (JJA) BSA record as well as the mean summer (JJA) NAO index each year during the period 2001-2016.
The original legend on the lower panel of Figure 8 (now Figure 9 not include the NAO index. This may have been a source of confusion. For clarification, the legend has been modified to incl the NAO index (black line) and a reference to Section 3.3 where graph is discussed, has been added.

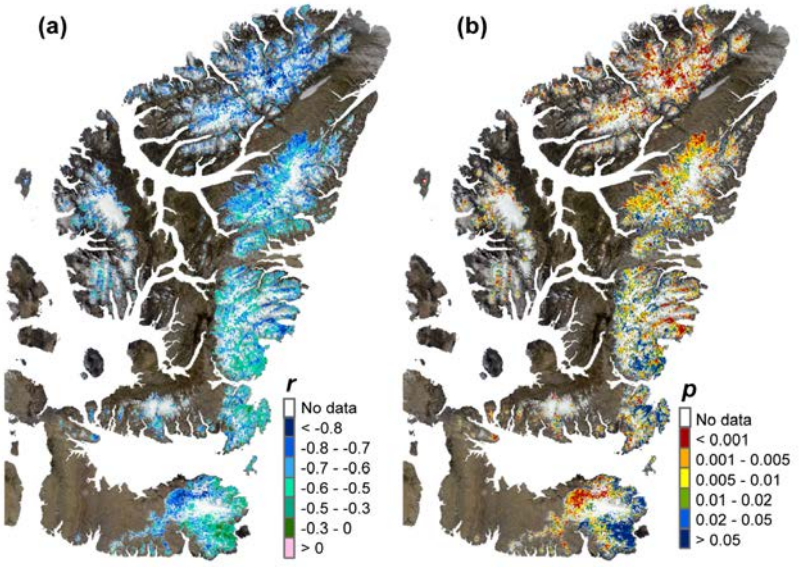
(a)
(b)
r
No data
< -0.8
-0.8 - -0.7
-0.7 - -0.6
-0.6 - -0.5
-0.5 - -0.3
-0.3 - 0
> 0
p
No data
< 0.001
0.001 - 0.005
0.005 - 0.01
0.01 - 0.02
0.02 - 0.05
> 0.05

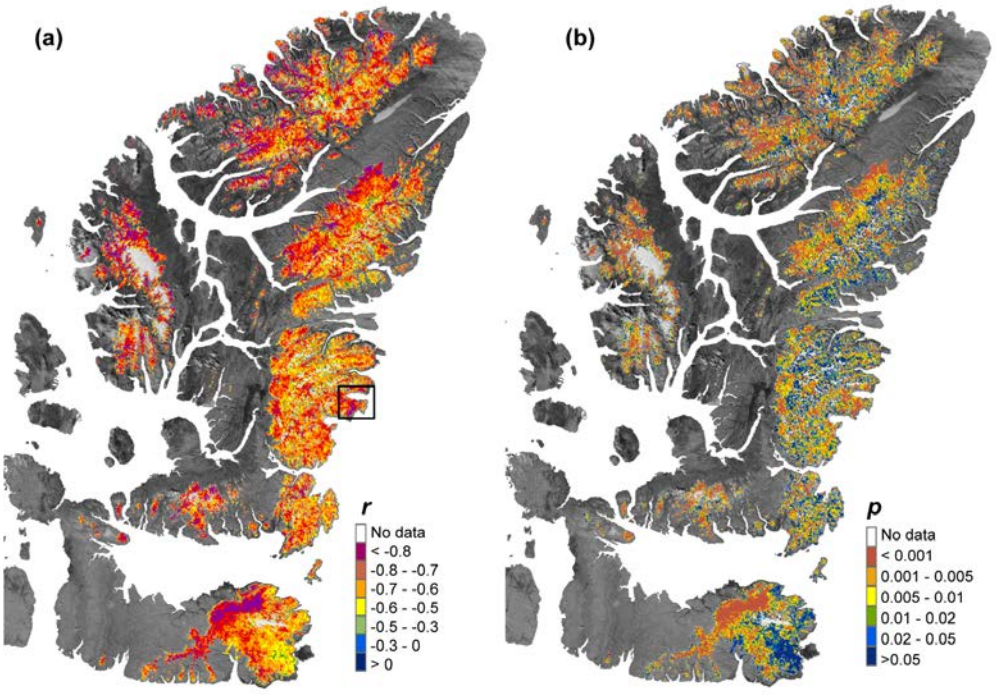

Figure 910: (a) Pearson Correlation Coefficient (r) and (b) p-value for linear regression of the 16 year BSA and LST record. ~~**Black box shows location of Cadogan Inlet (Sect. 4.2).**~~ Background image: MODIS 4 July 2011., ~~B~~brown indicates non-glaciated land cover.